ORIGINAL ARTICLE



Check for updates

An exploratory steady-state redox model of photosynthetic linear electron transport for use in complete modelling of photosynthesis for broad applications

Lianhong Gu¹ | Bernard Grodzinski² | Jimei Han³ | Telesphore Marie² | Yong-Jiang Zhang⁴ | Yang C. Song⁵ | Ying Sun³ |

Correspondence

Lianhong Gu, Oak Ridge National Laboratory, Environmental Sciences Division and Climate Change Science Institute, Oak Ridge, TN 37831, USA.

Email: lianhong-gu@ornl.gov

Funding information

US Department of Energy Office of Science

Abstract

A photochemical model of photosynthetic electron transport (PET) is needed to integrate photophysics, photochemistry, and biochemistry to determine redox conditions of electron carriers and enzymes for plant stress assessment and mechanistically link suninduced chlorophyll fluorescence to carbon assimilation for remotely sensing photosynthesis. Towards this goal, we derived photochemical equations governing the states and redox reactions of complexes and electron carriers along the PET chain. These equations allow the redox conditions of the mobile plastoquinone pool and the cytochrome b₆f complex (Cyt) to be inferred with typical fluorometry. The equations agreed well with fluorometry measurements from diverse C₃/C₄ species across environments in the relationship between the PET rate and fraction of open photosystem Il reaction centres. We found the oxidation of plastoquinol by Cyt is the bottleneck of PET, and genetically improving the oxidation of plastoquinol by Cyt may enhance the efficiency of PET and photosynthesis across species. Redox reactions and photochemical and biochemical interactions are highly redundant in their complex controls of PET. Although individual reaction rate constants cannot be resolved, they appear in parameter groups which can be collectively inferred with fluorometry measurements for broad applications. The new photochemical model developed enables advances in different fronts of photosynthesis research.

KEYWORDS

cytochrome b₆f complex, photosynthesis model, photosystems, plastoquinone, redox reactions

1 | INTRODUCTION

Photosynthesis is commonly divided into two stages of broad reactions—the light (or light-dependent) reactions and the carbon (also known as dark, light-independent, or Calvin-Benson cycle)

reactions (Buchanan, 2016). From a system modelling point of view, it is much more insightful to divide photosynthesis into three stages of reactions or three eras based on the characteristic time scales of consecutive photosynthetic events. The three-stage separation was first proposed by Kamen (1963) and shown in Figure 1 with

This is an open access article under the terms of the Creative Commons Attribution-NonCommercial License, which permits use, distribution and reproduction in any medium, provided the original work is properly cited and is not used for commercial purposes.

© 2023 The Authors. Plant, Cell & Environment published by John Wiley & Sons Ltd.



¹Oak Ridge National Laboratory, Environmental Sciences Division and Climate Change Science Institute, Oak Ridge, Tennessee, USA

²Department of Plant Agriculture, University of Guelph, Guelph, Ontario, Canada

³School of Integrative Plant Science, Cornell University, Ithaca, New York, USA

⁴School of Biology and Ecology, University of Maine, Orono, Maine, USA

⁵Department of Hydrology and Atmospheric Sciences, University of Arizona, Tucson, Arizona, USA

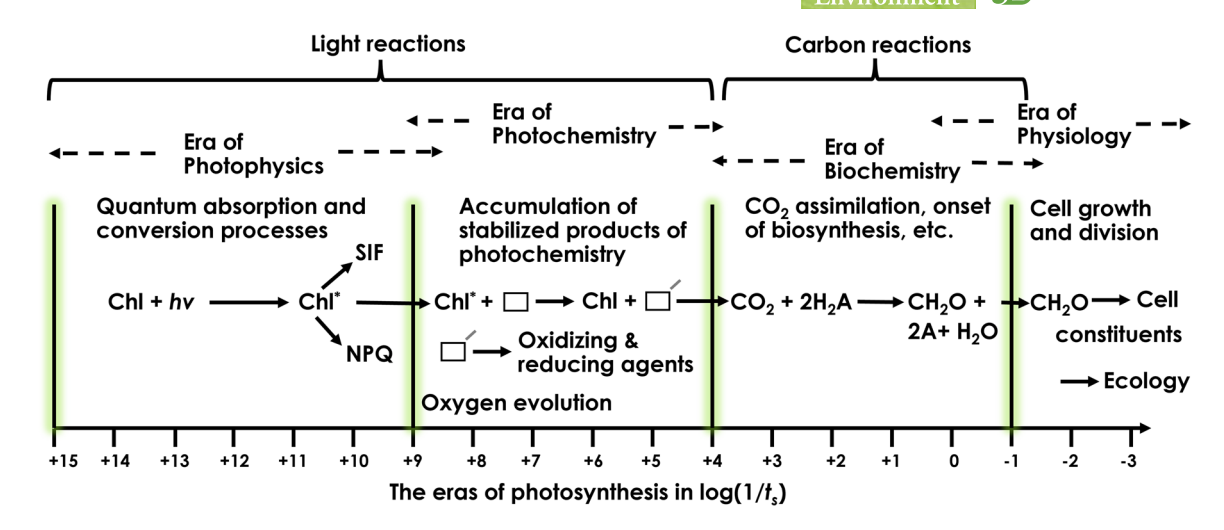


FIGURE 1 The Eras of Photosynthesis, modified from Kamen (1963). The time t_s is expressed in seconds. See the text in Introduction for explanation.

modifications—the eras (reactions) of photophysics, photochemistry, and biochemistry. These three eras are then followed by the eras of physiology and ecology.

In the Kamen division of photosynthesis, the light reactions are further partitioned into the photophysical reactions and photochemical reactions because these two groups of reactions are spatially separated, follow different laws, and operate at vastly contrasting time scales. The photophysical reactions cover the stages of light harvesting in the antenna complexes and the transfer of excitation energy to the reaction centres of photosystem II (PSII) and photosystem I (PSI). These reactions are governed by physical principles such as quantum mechanics, energy conservation, and Förster resonance energy transfer, and occur at a characteristic time scale of pico- to nanoseconds (Amarnath et al., 2016). It is within the photophysical reactions that fluorescence, whether passive (e.g., suninduced chlorophyll fluorescence or SIF) or active (e.g., pulse amplitude modulated (PAM) fluorometry), is emitted. The mechanisms that regulate nonphotochemical quenching (NPQ) depend on feedbacks from later stages of photosynthesis and can be slow. However, NPQ competes for the dissipation of excitation energy of the singlet states in the light harvesting antenna complexes before the excitation reaches the reaction centres for photochemistry. Thus, NPQ also occurs during the photophysical reactions.

The photochemical reactions cover the subsequent electron transport. This era includes water splitting in the oxygen evolving complex, charge separation, acquiring of electrons by acceptors in the reaction centres, and transfer of electrons by mobile carriers either within the lipid bilayer core of thylakoid membrane, lumen, or stroma to the eventual acceptor NADP+ to produce NADPH in the stroma to be used in the biochemical (carbon) reactions. It also encompasses electron exchanges within the cytochrome b₆f complex (Cyt), proton pumping across the thylakoid membrane, and synthesis. The photochemical reactions are of reduction-oxidation (redox) nature, and governed by thermodynamics, electrochemistry, and chemiosmotic theory. The fastest processes are the charge separation and water splitting while the slowest is the diffusion of mobile electron carriers; as a result, the photochemical reactions operate at a characteristic time scale of nano- to milli-seconds. A natural boundary between the photophysical and photochemical reactions is the charge separation in the reaction centres, which serves as an excitation energy trap and initiates a chain of redox reactions. This boundary is not clear-cut as photosynthetic units are interconnected, excitation can be redirected from closed to open reaction centres, and some photophysical processes such as state transition may be affected by redox status of components of the electron transport chain (Allen, 2002). Also, the photophysical and photochemical reactions cannot be discussed or modelled without considering each other. Nevertheless, separating the light reactions into photophysical and photochemical parts facilitates model formulation.

The ATP and NADPH produced at the end of photochemical reactions are used in the biochemical (carbon) reactions to reduce CO₂ to form sugar. Because the carbon reactions exactly overlap with the era of biochemistry in the Kamen division, we will use the phrase 'biochemical reactions' interchangbly with the carbon reactions. Among the three stages of reactions of photosynthesis, the photophysical and biochemical reactions are much better studied than the photochemical reactions. In both field and laboratory conditions, the photophysical reactions are routinely monitored with fluorometry techniques (Baker, 2008) whereas gas exchange measurements are commonly made for probing the biochemical reactions (Long and Bernacchi, 2003). In contrast, it is difficult to monitor the photochemical reactions, particularly the redox reactions between transmembrane protein complexes and electron carriers.

A vast number of models of photophysical, photochemical and biochemical reactions have been developed with varying degrees of complexity, depending on their specific applications (Stirbet et al., 2020). These models range from partial process representations (e.g., using quantum mechanics to model light harvesting in photosystems, Amarnath et al., 2016; Wang et al., 2018) to

3653040, 2023, 5, Downloaded from https://onlinelibrary.wiley.com/doi/10.1111/pce.14563, Wiley Online Library on [29/12/2023]. See the Terms and Conditions (https://onlinelibrary.wiley.com/ecrms-and-conditions) on Wiley Online Library for rules of use; OA articles are governed by the applicable Creative Commons

attempts of full system integration (e-photosynthesis) with dozens or even hundreds of ordinary differential equations (Laisk et al., 2006; Zhu et al., 2013). Models of broad applications are generally simplified and stead-state and can be directly related to measurable variables. The most successful photosynthesis model is perhaps the Farquhar-von Caemmerer-Berry (FvCB) biochemical model of photosynthesis (Farquhar et al., 1980; Sharkey, 1985). The FvCB model simulates the steady-state carbon metabolism of the Calvin-Benson cycle and can be readily parameterized and validated with leaf gas exchange measurements. As a result, the FvCB model has dominated the photosynthesis and carbon cycle modelling for the last several decades. Although the FvCB model mechanistically represents the energy demands of the Calvin-Benson and photorespiratory cycles as well as the Michaelis-Menten kinetics of Rubisco, it is not a complete model of photosynthesis (Farquhar et al., 2001). It contains neither photophysical nor photochemical mechanisms and cannot be used directly in studies where light reactions must be explicitly considered. For example, the FvCB model has had very limited applications in analyzing fluorometry measurements, which are as widely made and as important for photosynthesis research as gas exchange measurements. Also, important eco-physiological impacts of issues such as light harvesting, excitation energy dissipation, and regulation of electron transport cannot be analyzed with the FvCB model. To enable such studies, models of photophysical and photochemical reactions at similar levels of complexity, mechanistic representation, and readiness for parameterization and testing must be developed and coupled with the FvCB model.

Gu et al. (2019) developed a photophysical model to quantify the excitation energy dissipation pathways as a function of the fraction of open photosystem II (PSII) reaction centres under the lake model (q_L) and NPQ. Both q_L and NPQ can be measured with pulse-amplitude modulated (PAM) fluorometry (Baker, 2008). According to this model, the linear electron transport rate (J_{PSII}) from PSII to photosystem I (PSI) is determined by the photosynthetically active radiation (PAR) according to the following equation:

$$J_{\text{PSII}} = \frac{\beta \alpha \text{PAR}}{\frac{1 + NPQ}{q_L} \times \frac{1 - \Phi_{\text{PSIImax}}}{\Phi_{\text{PSIImax}}} + 1},$$
 (1)

Here α is the leaf absorptance in PAR, β is the fraction of absorbed energy allocated to PSII, NPQ is the parameter of NPQ, and $\Phi_{PSIImax}$ is the maximum photochemical quantum yield of PSII. In the context of PAM fluorometry data analysis, Equation (1) is essentially a restatement of the expression that relates q_L to NPQ as derived in Miyake et al. (2009). But as shown later, Equation (1) points to the direction of coupled modelling of photophysics, photochemistry and biochemistry of photosynthesis. Gu et al. (2019) also derived a corresponding equation for SIF emission, providing a mechanistic basis to remotely sense vegetation physiology by observing SIF. The photophysical model of Gu et al. (2019) is compatible with FvCB in complexity and mechanistic rigorousness, which is important for practical applications.

In theory, the FvCB model predicts the electron transport rate that is used to support CO₂ assimilation, not the whole chain electron transport rate J_{PSII}, a small fraction of which also flows to other synthetic processes such as nitrate reduction and photoreduction of O₂. Nevertheless, the electron transport rate calculated from CO₂ assimilation is highly linearly correlated with J_{PSII} calculated from PAM fluorometry (von Caemmerer, 2000). If alternative electron sinks are accounted for, the FvCB model can be used to predict J_{PSII} from environmental variables. However, the FvCB model and Equation 1 do not form a closed system because FvCB, as a biochemical model, predicts neither q_L nor NPQ. To form a closed system, a third independent model is needed. A nonideal approach is to empirically parameterize q_i or NPQ to close the system. Using an empirical approach and assuming alternative electron sinks are negligible, it has been shown that the joint use of the photophysical model of Gu et al. (2019) with FvCB can lead to insights on how SIF can be applied effectively to infer photosynthesis (Han, Chang, et al., 2022) and how the information contained in SIF with respect to photosynthetic capacities depends on the redox state of PSII (Han, Gu, et al., 2022). These studies show the promises of coupled models of light reactions and FvCB for large-scale photosynthesis research. However, to advance further, a more robust solution is needed to enable a mechanistic coupling of the photophysical model of Gu et al. (2019) with FvCB.

This solution is logically provided by modelling the photochemical reactions, which is the bridge between the photophysical reactions, modelled by Gu et al. (2019), and the biochemical reactions, modelled by FvCB. Since the publication of Gu et al. (2019), we have been working to develop such a photochemical model. Although our initial aim was to enable mechanistically modelling SIF emission and its relationship with gross primary production (GPP), a photochemical model of photosynthesis can have much broader applications. During photosynthesis, PSII and PSI must coordinate in photon harvesting, excitation transfer, and redox reactions to complete the linear electron transport (LET) from the ultimate donor (water) at the PSII end to the eventual acceptor (NADP+) at the PSI end. A series of redox reactions along the electron transport chain control LET and are regulated by a myriad of feedforward and feedback processes to ensure that the supply of electron transport products (e.g., NADPH and ATP) is in balance with the demand of biochemical reactions (Foyer et al., 2012; Rochaix, 2011). Many previous researchers have modelled LET, often in the context of simulating the rapid or slow chlorophyll fluorescence induction curves (e.g., Ebenhöh et al., 2011; Laisk et al., 2006; Lazár, 2013; Loriaux et al., 2013; Zhu et al., 2005, 2013). The complexities of these models depend on how the reaction centres are represented and how many redox reaction events are considered. They use ordinary differential equations to describe the temporary variations of redox reagent pool sizes (states) and the fluxes between them. These models are useful for modelling transient dynamics to understand specific processes in the photosynthetic system at short time scales (e.g., ~seconds) and for revealing insights on how certain reactions can be optimized to increase photosynthetic

3633040, 2023, 5, Downloaded from https://onlinelibrary.wiley.com/doi/10.1111/pce.14563, Wiley Online Library on [29/12/2023]. See the Terms and Conditions (https://onlinelibrary.wiley.com/terms-and-conditions) on Wiley Online Library for rules of use; OA articles are governed by the applicable Creative Commons Licenses.

efficiency (e.g., Zhu et al., 2007). However, they generally contain numerous parameters, many of which cannot be readily available at the leaf scale in field conditions, making them difficult for broad applications at large scales.

In this study, we will build upon the previous modelling efforts of photochemical reactions of Zhu et al. (2005), Laisk et al. (2006), Ebenhöh et al. (2011), Lazár (2013), Loriaux et al. (2013), and Zhu et al. (2013), and a new theory that explains the structure and function of granal thylakoid of higher plants (Gu et al., 2022). We solve the coupled systems of state equations at the steady state to derive concise, easy-to-use redox relationships between the linear electron transport rate (J_{PSII}, major symbols and abbreviations are defined in Table 1), the fraction of open PSII reaction centres (q), the fraction of the plastoquinone (PQ) pool that is oxidized (denoted by h_{PO}), and the fraction of Cyt that is available for LET (denoted by h_{cyt}). Because both J_{PSII} and q can be measured with PAM fluorometry, the obtained J_{PSII} -q relationships can be used to infer redox reaction parameters which in turn can be used to calculate h_{PO} and h_{cvt} at the leaf level. To our knowledge, these quantitative relationships have never been reported previously. Additionally, we will show that the thylakoid ultrastructural dynamics, which have been experimentally observed (Höhner et al., 2020; Kirchhoff et al., 2011; Li et al., 2020) but generally ignored in previous non-steady state models, appear to be crucial to modelling photosynthetic electron transport at the leaf scale and require more in-depth investigations.

To avoid confusion and misunderstanding, we must point out, at the very beginning, that the photochemically defined J_{PSII} -q relationships, which are to be derived below, are related but independent to the photophysically defined J_{PSII} -q relationship as shown in Equation (1). Equation (1) applies to processes that occur before the excitation energy reaches PSII whereas the photochemical J_{PSII} -q relationships to be introduced later apply to processes that occur along the electron transport chain, after the excitation energy has been delivered to PSII. Further, to understand the rest of the paper, one must keep in mind the three-stage separation of photosynthesis (photophysics, photochemistry and biochemistry, Figure 1) and that this present study focuses on the middle stage (photochemistry). Also, we need to be aware the energy form in photophysics is excitation (i.e., the transfer of electron from a lower energy state to a higher energy state but in both states, electron is still bound) while in photochemistry, the energy form is electron transport and proton translocation. More clarifications will be provided later when the photochemical equations are given.

As intended and shown later, the obtained photochemical relationships are indeed compatible in complexity and mechanistic rigorousness with the models of Gu et al. (2019) and FvCB, and thus can be coupled with them to conduct integrated modelling of photophysics, photochemistry, and biochemistry of photosynthesis for general applications. Future studies will report on this photophysical-photochemical-biochemical coupling, and on the mechanistic modelling of SIF. The development of approaches to inferring h_{PO} and h_{cvt} with PAM fluorometry under natural conditions also represents significant advancements. The redox state of PQ pool

acts as a sensor of environmental conditions (Wilson et al., 2006), modulates the expression of genes encoding the light-harvesting complexes (Escoubas et al., 1995), and regulates state transition through which the relative antenna sizes of PSII and PSI are adjusted in response to variations in light intensity to ensure the excitation balance between the two photosystems (Allen, 2002). Cyt is strategically located in the centre of the electron transport chain (ETC), catalyzes LET, cyclic electron transport (CET), and proton pumping from the stroma to lumen, and plays a key role in steadystate photosynthesis (J. E. Johnson and Berry, 2021; Tikhonov, 2014). However, these processes have not been adequately studied so far because it is difficult to measure the redox states of the PQ pool and Cyt of a leaf in situ. The photochemical models developed in this study offer a potential to gain such vital information via the easily measured J_{PSII} and q, and thus facilitate studying the regulations of state transitions and electron transport by the redox states of PQ and Cyt under varying environmental conditions. We will use PAM fluorometry measurements collected from a large number of C₃/C₄ species in different climates to test the steady-state photochemical models. Future research priorities and model components that still require further independent testing will be identified.

THEORETICAL DERIVATIONS OF THE STEADY-STATE PHOTOCHEMICAL MODELS

Strategy 2.1

We seek a balance between the desire to rigorously represent the fundamental processes along the photosynthetic ETC and the need to ensure all model parameters can be realistically constrained by commonly available leaf-level measurements (e.g., PAM fluorometry with typical light, CO₂, and temperature responses). This balance is unlikely to be achieved if the whole ETC is modelled even if only the main players, for example, PSII, PQ, Cyt, plastocyanin (PC), PSI and ferredoxin (Fd), are included in the state equations. If the whole ETC is not modelled, then an option can be decided whether to focus the modelling effort on the front end (PSII) or the rear end (PSI) of the ETC. In steady state, LET through PSII and PSI should be the same and thus either option could potentially work. In theory, it is possible to model ETC with a focus on PSI (J. E. Johnson and Berry, 2021). However, a focus on PSII has two clear advantages. First, PSII contributes to variable fluorescence much more than PSI does (Lazár, 2013), and using absorbance changes to infer PSI redox state requires deconvolutions of mixed signals from redox state changes in P700, PC and Fd (Schreiber and Klughammer, 2016). As a result, it is easier to monitor the redox state of PSII than that of PSI. In fact, leaf-level measurements on PSII are far more available than on PSI. Second, PSII turns over more slowly than PSI due to the need of replacing plastoquinone at the loosely bound (Q_B) site (Caffarri et al., 2014) and thus the front section of ETC controls the overall performance of the whole chain.

 TABLE 1
 List of frequently used symbols and abbreviations.

Symbol	Definition	Units
Α	Acceptor when given in normal	NA
A (Q _A Q _B model)	The concentration of photosystem II with both the tightly bound and loosely bound plastoquinone in the ground state, when italicized	μmol m ⁻²
B (Q _A Q _B model)	The concentration of photosystem II with the tightly bound plastoquinone in the ground state and the loosely bound plastoquinone singly reduced, when italicized	$\mu mol m^{-2}$
C (OC model)	The concentration of photosystem II with closed reaction centre, when italicized	$\mu mol m^{-2}$
C (Q _A Q _B model)	The concentration of photosystem II with the tightly bound plastoquinone in the ground state and the loosely bound plastoquinone doubly reduced, when italicized	$\mu mol m^{-2}$
D	Donor when given in normal	NA
D (Q _A Q _B model)	The concentration of photosystem II with a reduced tightly bound plastoquinone and a ground-state loosely bound plastoquinone, when italicized	$\mu mol m^{-2}$
E (Q _A Q _B model)	The concentration of photosystem II with a reduced tightly bound plastoquinone and a singly reduced loosely bound plastoquinone, when italicized	$\mu mol m^{-2}$
F (Q _A Q _B model)	The concentration of photosystem II with a reduced tightly bound plastoquinone and a doubly reduced loosely bound plastoquinone, when italicized	$\mu mol m^{-2}$
I (PSII state)	The concentration of nonreversible photosystem II reaction centres—permanently inhibited state of reaction centres that are incapable of doing photochemistry, including the inhibited PSII, Q _B -nonreducing PSII and cushion PSII (lumped)	μmol m ⁻²
O (OC model)	The concentration of photosystem II with open reaction centre, when italicized	$\mu molm^{-2}$
PAR	The incident photosynthetically active radiation	$\mu molm^{-2}s^{-1}$
a_q	The redox poise stoichiometry parameter between cytochrome $b_{\text{o}}f$ complex and photosystem II	NA
b_s	The parameter controlling the speed of light-induced thylakoid swelling/shrinking with value given on the basis of absorbed photosynthetically active radiation allocated to photosystem II	μmol ⁻¹ m ² s
Cs	The parameter determining the maximum impact of macromolecular crowding on electron transport via the redox dynamics of cytochrome $b_6 f$ complex	NA
CET	Cyclic electron transport	
Cyt	The cytochrome b ₆ f complex	
D	The first-order rate constant for the back transfer of electron from the acceptor to the donor	s ⁻¹
Eτ	The composite temperature sensitivity parameter in the standardized temperature response function of electron transport derived from the Marcus theory, related to free energy of activation	К
ETC	Electron transport chain	
f_s	The light-induced thylakoid swelling and shrinking function	NA
f_q	The redox poise balance function between cytochrome $\mathrm{b}_{\mathrm{6}}\mathrm{f}$ complex and photosystem II	NA
f_T	The standardized temperature response function of electron transport in proteins according to the Marcus theory	NA
Н	The concentration (pool size) of plastoquinol	$\mu molm^{-2}$
H _{AD}	The quantum mechanical electronic coupling between the initial and final (donor and acceptor) states	J
h _{cyt}	Fraction of cytochrome b ₆ f complex available for linear electron transport	NA
h_{PQ}	Fraction of the mobile plastoquinone pool that is oxidized	NA
h _{PQH2}	Fraction of the mobile plastoquinone pool that is reduced, =1 - h_{PQ}	NA



TABLE 1 (Continued)

The gross excitation energy flux received by photosystem II with both the tightly bound and loosely bound plastoquinone are gry flux received by photosystem II with both the tightly bound and loosely bound plastoquinone in the ground state and the loosely bound plastoquinone in the ground state and the loosely bound plastoquinone in the singly reduced state. The excitation energy flux received by photosystem II with the tightly bound plastoquinone in the ground state and the loosely bound plastoquinone in the singly reduced state. The excitation energy flux received by photosystem II with the tightly bound plastoquinone in the ground state and the loosely bound plastoquinone in the doubly reduced state. The first-order rate constant for the transfer of electron from the reduced Q _A to the ground state Q _B and for the reverse reaction, respectively. Kanz and kanz. The first-order rate constant for the transfer of electron from the reduced Q _A to the singly reduced Q _B and for the reverse reaction, respectively. Kanz and kanz. The first-order rate constant for the transfer of electron from the reduced Q _A to the singly reduced Q _B and for the reverse reaction, respectively. Kanz and kanz. The first-order rate constant for the transfer of electron from the reduced Q _A to the singly reduced Q _B and for the reverse reaction, respectively. Kanz and kanz. The first-order rate constant for the transfer of electron from the reduced Q _A to the singly reduced Q _B and for the reverse reaction, respectively. Kanz and kanz. The first-order rate constant for the transfer of electron from the reduced Q _A to the singly reduced Q _B and for the reverse reaction, respectively. Kanz and kanz. The first-order rate constant for the transfer of electron from the reduced Q _A to the singly reduced Q _B and for the reverse reaction, respectively. Kanz and kanz. The first-order rate constant for the transfer of electron from the reduced Q _A to the single value of the single value of the single value of the s	Symbol	Definition	Units
The excitation energy flux received by photosystem II with both the tightly bound and loosely bound plastoquinone plastoquinone in the excitation energy flux received by photosystem II with the tightly bound plastoquinone in the ground state and the loosely bound plastoquinone in the singly reduced state The excitation energy flux received by photosystem II with the tightly bound plastoquinone in the ground state and the loosely bound plastoquinone in the doubly reduced state The first-order rate constant for the transfer of electron from the reduced Q _A to the ground state Q _B and for the reverse reaction, respectively First-order rate constant for the transfer of electron from the reduced Q _A to the singly reduced Q _B and for the reverse reaction, respectively First-order rate constant for the transfer of electron from the reduced Q _A to the singly reduced Q _B and for the reverse reaction, respectively First Produced State First Produced Q _B and for the reverse reaction, respectively First Produced Q _B and for the reverse reaction, respectively First Produced Q _B and for the reverse reaction, respectively First Produced Q _B and for the reverse reaction, respectively First Produced Q _B and for the reverse reaction, respectively First Produced Q _B and for the reverse reaction, respectively First Produced Q _B Produced Produced Q _B Produced Prod	J_{PSII}	The linear electron transport rate from photosystem II to I	μ mol m ⁻² s ⁻¹
The excitation energy flux received by photosystem II with the tightly bound plastoquinone in the ground state and the loosely bound plastoquinone in the singly reduced state The excitation energy flux received by photosystem II with the tightly bound plastoquinone in the ground state and the loosely bound plastoquinone in the doubly reduced state First-order rate constant for the transfer of electron from the reduced QA to the ground state QB and for the reverse reaction, respectively First-order rate constant for the transfer of electron from the reduced QA to the ground state QB and for the reverse reaction, respectively First-order rate constant for the transfer of electron from the reduced QA to the ground state QB and for the reverse reaction, respectively First QB Boltzmann constant First QB Boltzmann Co	J _G *	The gross excitation energy flux	$\mu mol\ m^{-2}\ s^{-1}$
plastoquinone in the ground state and the loosely bound plastoquinone in the singly reduced state The excitation energy flux received by photosystem II with the tightly bound plastoquinone in the ground state and the loosely bound plastoquinone in the doubly reduced state Kaes and Kaes	J _A *		μ mol m ⁻² s ⁻¹
plastoquinone in the ground state and the loosely bound plastoquinone in the doubly reduced state Kasa and kasat The first-order rate constant for the transfer of electron from the reduced Q _A to the ground state Q _B and for the reverse reaction, respectively Kasa and kasa2 The first-order rate constant for the transfer of electron from the reduced Q _A to the singly reduced Q _B and for the reverse reaction, respectively Kasa = k _{AB1} /K _{AB2} NA NA Boltzmann constant Ket The rate constant of electron transport in proteins according to the Marcus theory s ⁻¹ **K _{PSII} = k _{AB1} /N _{PSII} #*K _{PSII} = k _{AB1} /N _{PSII} NA NA LET Linear electron transport NPQ Nonphotochemical quenching N _{PSII} The foliar concentrations of total photosystem II reaction centres per unit leaf area µmol m ⁻² N _{PSII} The foliar concentration of the free plastoquinone and plastoquinol pool per unit leaf area µmol m ⁻² **Nort The foliar concentration of the cytochrome b _d complex available (uninhibited) for linear electron transport per unit leaf area Nort The total foliar concentration of the tree plastoquinone PAM Pulse amplitude modulated PAR Photosynthetically active radiation PC Plastocyanin PQ Free plastoquinone PGC Plastocyanin PQ Free plastoquinone PGC Plastocyanin PQ Free plastoquinone PGC Plastocyanin PG Fraction of open photosystem I reaction centres under the lake connectivity of photosynthetic units NA Fraction of open PSII reaction centres under the puddle connectivity of photosynthetic units NA Fraction of open PSII reaction centres under the puddle connectivity of photosynthetic units NA Fraction of open PSII reaction centres under the puddle connectivity of photosynthetic units	J _B *	plastoquinone in the ground state and the loosely bound plastoquinone in the singly	μ mol m ⁻² s ⁻¹
ground state Q _B and for the reverse reaction, respectively The first-order rate constant for the transfer of electron from the reduced Q _A to the singly reduced Q _B and for the reverse reaction, respectively NA Re Boltzmann constant J K 1 Ker The rate constant of electron transport in proteins according to the Marcus theory s 1 ke _{BBI} = k _{AB1} /k _{AB2} Ke _{BBI} = k _{AB1} /k _{AB1} MA Ke _{BBI} = k _{AB2} /k _{AB2} MA Ke _{BBI} = k _{BA2} /k _{AB2} NA Lier Linear electron transport Nonphotochemical quenching Nonphotochemical quenching Ne _{BBI} The foliar concentrations of total photosystem II reaction centres per unit leaf area µmol m ⁻² Me _{BBI} Protogram The foliar concentration of the replastoquinone and plastoquinol pool per unit leaf area µmol m ⁻² Me _{BBI} The foliar concentration of the cytochrome bg complex available (uninhibited) for linear electron transport per unit leaf area µmol m ⁻² Me _{BBI} The total foliar concentration of the cytochrome bg complex, including both uninhibited µmol m ⁻² Me _{BBI} The total foliar concentration of the cytochrome bg complex, including both uninhibited µmol m ⁻² Me _{BBI} The total foliar concentration of the cytochrome bg complex, including both uninhibited µmol m ⁻² Me _{BBI} Protosystem on the cytochrome bg complex including both uninhibited µmol m ⁻² Me _{BBI} Protosynthetically active radiation µmol m ⁻² Protosynthetic NA Praction of open polotosystem reaction centres under the lake connectivity of photosynthetic units NA Praction of open PSII reaction centres under the puddle connectivity of photosynthetic units NA Praction of open PSII reaction centres under the puddle connectivity of photosynthetic NA Praction of open PSII	J _Č	plastoquinone in the ground state and the loosely bound plastoquinone in the doubly	μ mol m ⁻² s ⁻¹
singly reduced Q _B and for the reverse reaction, respectively kaB	k_{AB1} and k_{BA1}		s ⁻¹
Boltzmann constant ArT The rate constant of electron transport in proteins according to the Marcus theory F1 ArT The rate constant of electron transport in proteins according to the Marcus theory F1 ArS ArS ArS ArS ArS ArS ArS ArS ArS Ar	k_{AB2} and k_{BA2}		s ⁻¹
The rate constant of electron transport in proteins according to the Marcus theory **I** **Repul*** **Repul** *** *** *** *** *** *** ***	k _{AB}	$= k_{AB1}/k_{AB2}$	NA
ke _{SII}	k _B	Boltzmann constant	J K ⁻¹
$k_1 = k_{BA1}/k_{AB1}$ NA $k_2 = k_{BA2}/k_{AB2}$ NA LET Linear electron transport NPQ Nonphotochemical quenching NPSII The foliar concentrations of total photosystem II reaction centres per unit leaf area μ mol m ⁻² NPQ _T The foliar concentration of the free plastoquinone and plastoquinol pool per unit leaf area μ mol m ⁻² NPSII The foliar concentration of the cytochrome $b_a f$ complex available (uninhibited) for linear electron transport per unit leaf area NPSII The total foliar concentration of the cytochrome $b_a f$ complex, including both uninhibited and inhibited complexes for linear electron transport per unit leaf area OEC Oxygen evolving complex P The concentration (pool size) of free plastoquinone PAM Pulse amplitude modulated PAR Photosynthetically active radiation PQ Free plastoquinone PQ Pastocyanin PQ Free plastoquinone PQH ₂ Plastoquinol PSI Photosystem I PSI Photosystem I PSI Photosystem I PFaction of open photosystem reaction centres under the lake connectivity of photosynthetic units NA Praction of open PSII reaction centres under the puddle connectivity of photosynthetic units NA	k _{ET}	The rate constant of electron transport in proteins according to the Marcus theory	s ⁻¹
LET Linear electron transport NPQ Nonphotochemical quenching NPSSII The foliar concentrations of total photosystem II reaction centres per unit leaf area µmol m ⁻² NPQT The foliar concentration of the free plastoquinone and plastoquinol pool per unit leaf area µmol m ⁻² The foliar concentration of the cytochrome b _o f complex available (uninhibited) for linear electron transport per unit leaf area Nort The total foliar concentration of the cytochrome b _o f complex, including both uninhibited and inhibited complexes for linear electron transport per unit leaf area OEC Oxygen evolving complex P The concentration (pool size) of free plastoquinone µmol m ⁻² PAM Pulse amplitude modulated PAR Photosynthetically active radiation µmol m ⁻² s ⁻² PC Plastocyanin PQ Free plastoquinone PQH ₂ Plastoquinol PSI Photosystem I G Fraction of open photosystem reaction centres under the lake connectivity of photosynthetic units NA Praction of open PSII reaction centres under the puddle connectivity of photosynthetic units NA Praction of open PSII reaction centres under the puddle connectivity of photosynthetic units	k _{PSII}	$= k_{AB1} N_{PSII}$	$\mu mol\ m^{-2}\ s^{-1}$
LET Linear electron transport NPQ Nonphotochemical quenching The foliar concentrations of total photosystem II reaction centres per unit leaf area µmol m ⁻² The foliar concentration of the free plastoquinone and plastoquinol pool per unit leaf area µmol m ⁻² N _{PQT} The foliar concentration of the cytochrome b _a f complex available (uninhibited) for linear electron transport per unit leaf area N _{OrtT} The total foliar concentration of the cytochrome b _a f complex, including both uninhibited and inhibited complexes for linear electron transport per unit leaf area OEC Oxygen evolving complex P The concentration (pool size) of free plastoquinone µmol m ⁻² PAM Pulse amplitude modulated PAR Photosynthetically active radiation µmol m ⁻² s ⁻² PC Plastocyanin PC Plastocyanin PC Plastoquinol PSI Photosystem I PSII Photosystem I Fraction of open photosystem reaction centres NA Fraction of open PSII reaction centres under the lake connectivity of photosynthetic units NA Praction of open PSII reaction centres under the puddle connectivity of photosynthetic units	k ₁	$=k_{\rm BA1}/k_{\rm AB1}$	NA
NPQ Nonphotochemical quenching The foliar concentrations of total photosystem II reaction centres per unit leaf area μmol m ⁻² NPQT The foliar concentration of the free plastoquinone and plastoquinol pool per unit leaf area μmol m ⁻² The foliar concentration of the cytochrome b _δ f complex available (uninhibited) for linear electron transport per unit leaf area NCONT The total foliar concentration of the cytochrome b _δ f complex, including both uninhibited and inhibited complexes for linear electron transport per unit leaf area DEC Oxygen evolving complex P The concentration (pool size) of free plastoquinone μmol m ⁻² PAM Pulse amplitude modulated PAR Photosynthetically active radiation μmol m ⁻² s ⁻² PC Plastocyanin PC Plastocyanin PC Plastoquinol PPQ Free plastoquinone PPQH ₂ Plastoquinol PSI Photosystem I PSII Photosystem I Fraction of open photosystem reaction centres NA Praction of open PSII reaction centres under the lake connectivity of photosynthetic units NA Praction of open PSII reaction centres under the puddle connectivity of photosynthetic units	k ₂	$= k_{\text{BA2}}/k_{\text{AB2}}$	NA
NPSII The foliar concentrations of total photosystem II reaction centres per unit leaf area μmol m ⁻² NPQT The foliar concentration of the free plastoquinone and plastoquinol pool per unit leaf area μmol m ⁻² NevIL The foliar concentration of the cytochrome b _o f complex available (uninhibited) for linear electron transport per unit leaf area μmol m ⁻² NoVIT The total foliar concentration of the cytochrome b _o f complex, including both uninhibited and inhibited complexes for linear electron transport per unit leaf area μmol m ⁻² OEC Oxygen evolving complex μmol m ⁻² P The concentration (pool size) of free plastoquinone μmol m ⁻² PAM Pulse amplitude modulated μmol m ⁻² s ⁻² PPC Plastocyanin μmol m ⁻² s ⁻² PPC Plastoquinone μmol m ⁻² s ⁻² PPQ Free plastoquinone POHtosystem I PPSI Photosystem I Photosystem I PPSII Photosystem I NA QL Fraction of open Poll reaction centres under the lake connectivity of photosynthetic units NA QL Fraction of open PSII reaction centres under the puddle connectivity of photosynthetic units NA	LET	Linear electron transport	
NPQT The foliar concentration of the free plastoquinone and plastoquinol pool per unit leaf area μmol m ⁻² Nevt The foliar concentration of the cytochrome b ₆ f complex available (uninhibited) for linear electron transport per unit leaf area μmol m ⁻² NevtT The total foliar concentration of the cytochrome b ₆ f complex, including both uninhibited and inhibited complexes for linear electron transport per unit leaf area μmol m ⁻² OEC Oxygen evolving complex μmol m ⁻² P The concentration (pool size) of free plastoquinone μmol m ⁻² PAM Pulse amplitude modulated μmol m ⁻² s ⁻² PAR Photosynthetically active radiation μmol m ⁻² s ⁻² PC Plastocyanin PQ PQ Free plastoquinone PQH ₂ PQH ₂ Plastoquinol PPSI PSI Photosystem I PSI PSII Photosystem II Praction of open photosystem reaction centres NA qL Fraction of open PSII reaction centres under the lake connectivity of photosynthetic units NA qP Fraction of open PSII reaction centres under the puddle connectivity of photosynthetic units NA	NPQ	Nonphotochemical quenching	
The foliar concentration of the cytochrome b _o f complex available (uninhibited) for linear electron transport per unit leaf area N _{CytT} The total foliar concentration of the cytochrome b _o f complex, including both uninhibited and inhibited complexes for linear electron transport per unit leaf area OEC Oxygen evolving complex P The concentration (pool size) of free plastoquinone μmol m ⁻² PAM Pulse amplitude modulated PAR Photosynthetically active radiation μmol m ⁻² s ⁻² PC Plastocyanin PQ Free plastoquinone PQH ₂ Plastoquinol PSI Photosystem I PSI Photosystem I PFraction of open photosystem reaction centres NA Fraction of open PSII reaction centres under the lake connectivity of photosynthetic units NA Fraction of open PSII reaction centres under the puddle connectivity of photosynthetic units NA Praction of open PSII reaction centres under the puddle connectivity of photosynthetic units	N _{PSII}	The foliar concentrations of total photosystem II reaction centres per unit leaf area	$\mu mol m^{-2}$
electron transport per unit leaf area Note: The total foliar concentration of the cytochrome bef complex, including both uninhibited pmol m ⁻² and inhibited complexes for linear electron transport per unit leaf area OEC Oxygen evolving complex P The concentration (pool size) of free plastoquinone pulse PAM Pulse amplitude modulated PAR Photosynthetically active radiation plastoquinone plastocyanin PQ Free plastocyanin PQ Free plastoquinone PQH ₂ Plastoquinol PSI Photosystem I PSII Photosystem II Q Fraction of open photosystem reaction centres NA Fraction of open PSII reaction centres under the lake connectivity of photosynthetic units NA Fraction of open PSII reaction centres under the puddle connectivity of photosynthetic NA Praction of pen PSII reaction centres under the puddle connectivity of photosynthetic NA Praction of open PSII reaction centres under the puddle connectivity of photosynthetic NA Praction of open PSII reaction centres under the puddle connectivity of photosynthetic NA Praction of open PSII reaction centres under the puddle connectivity of photosynthetic NA PRACTICAL PARCE PLANT AREA PLANT	N_{PQ_T}	The foliar concentration of the free plastoquinone and plastoquinol pool per unit leaf area	$\mu mol\ m^{-2}$
and inhibited complexes for linear electron transport per unit leaf area OEC Oxygen evolving complex P The concentration (pool size) of free plastoquinone	N_{cyt_L}		$\mu mol m^{-2}$
The concentration (pool size) of free plastoquinone µmol m ⁻² PAM Pulse amplitude modulated PAR Photosynthetically active radiation µmol m ⁻² s ⁻² PC Plastocyanin PQ Free plastoquinone PQH ₂ Plastoquinol PSI Photosystem I PSI Photosystem I PSI Praction of open photosystem reaction centres NA q _L Fraction of open PSII reaction centres under the puddle connectivity of photosynthetic units NA Fraction of open PSII reaction centres under the puddle connectivity of photosynthetic units NA units	N_{cyt_T}	, , , , ,	$\mu mol m^{-2}$
PAM Pulse amplitude modulated PAR Photosynthetically active radiation μmol m ⁻² s ⁻² PC Plastocyanin PQ Free plastoquinone PQH ₂ Plastoquinol PSI Photosystem I PSII Photosystem II Fraction of open photosystem reaction centres NA Fraction of open PSII reaction centres under the lake connectivity of photosynthetic units NA Fraction of open PSII reaction centres under the puddle connectivity of photosynthetic units NA	OEC	Oxygen evolving complex	
PAR Photosynthetically active radiation µmol m ⁻² s ⁻² PC Plastocyanin PQ Free plastoquinone PQH ₂ Plastoquinol PSI Photosystem I PSII Photosystem II PSII Praction of open photosystem reaction centres NA Fraction of open PSII reaction centres under the lake connectivity of photosynthetic units NA Fraction of open PSII reaction centres under the puddle connectivity of photosynthetic units NA	P	The concentration (pool size) of free plastoquinone	$\mu mol \ m^{-2}$
PC Plastocyanin PQ Free plastoquinone PQH ₂ Plastoquinol PSI Photosystem I PSII Photosystem II Fraction of open photosystem reaction centres NA Fraction of open PSII reaction centres under the lake connectivity of photosynthetic units NA Fraction of open PSII reaction centres under the puddle connectivity of photosynthetic units NA Fraction of open PSII reaction centres under the puddle connectivity of photosynthetic units	PAM	Pulse amplitude modulated	
PQH ₂ Plastoquinone PQH ₂ Plastoquinol PSI Photosystem I PSII Photosystem II q Fraction of open photosystem reaction centres NA Fraction of open PSII reaction centres under the lake connectivity of photosynthetic units NA Fraction of open PSII reaction centres under the puddle connectivity of photosynthetic units NA Praction of open PSII reaction centres under the puddle connectivity of photosynthetic units	PAR	Photosynthetically active radiation	$\mu mol\ m^{-2}\ s^{-2}$
PQH ₂ Plastoquinol PSI Photosystem I PSII Photosystem II Fraction of open photosystem reaction centres NA Fraction of open PSII reaction centres under the lake connectivity of photosynthetic units NA Fraction of open PSII reaction centres under the puddle connectivity of photosynthetic units NA Fraction of open PSII reaction centres under the puddle connectivity of photosynthetic units	PC	Plastocyanin	
PSI Photosystem I PSII Photosystem II Praction of open photosystem reaction centres NA Fraction of open PSII reaction centres under the lake connectivity of photosynthetic units NA Fraction of open PSII reaction centres under the puddle connectivity of photosynthetic units NA Fraction of open PSII reaction centres under the puddle connectivity of photosynthetic units	PQ	Free plastoquinone	
PSII Photosystem II Fraction of open photosystem reaction centres NA Fraction of open PSII reaction centres under the lake connectivity of photosynthetic units NA Fraction of open PSII reaction centres under the puddle connectivity of photosynthetic units NA Fraction of open PSII reaction centres under the puddle connectivity of photosynthetic units	PQH ₂	Plastoquinol	
Fraction of open photosystem reaction centres NA Fraction of open PSII reaction centres under the lake connectivity of photosynthetic units NA Fraction of open PSII reaction centres under the puddle connectivity of photosynthetic units NA Traction of open PSII reaction centres under the puddle connectivity of photosynthetic units	PSI	Photosystem I	
Fraction of open PSII reaction centres under the lake connectivity of photosynthetic units NA Fraction of open PSII reaction centres under the puddle connectivity of photosynthetic units NA NA The transfer of the puddle connectivity of photosynthetic units	PSII	Photosystem II	
q _P Fraction of open PSII reaction centres under the puddle connectivity of photosynthetic NA units	q	Fraction of open photosystem reaction centres	NA
units	q _L	Fraction of open PSII reaction centres under the lake connectivity of photosynthetic units	NA
7r The fraction of reversible photosystem II reaction centres NA	q_P		NA
	q _r	The fraction of reversible photosystem II reaction centres	NA

TABLE 1 (Continued)

Symbol	Definition	Units
Q_A	The tightly bound plastoquinone	
Q_B	The loosely bound plastoquinone	
r_d and r_r	The second-order rate constant for the electron transfer from the reduced acceptor to PQ to form PQH_2 and for the reverse reaction, respectively	$m^2 \mu mol^{-1} s^{-1}$
R ₁	The first resistance of electron transport = r_r/r_d	NA
R_2	The second resistance of electron transport = uN_{cyt_T}/r_dN_{PSII}	NA
Т	Leaf temperature	К
T_{O}	Reference leaf temperature (=298.15-K)	К
U	The second-order rate constant for the oxidation of plastoquinol by the RieskeFeS protein of cytochrome $b_{d}f$ complex	$m^2 \mu mol^{-1} s^{-1}$
U	The maximum oxidation potential of free plastoquinone and plastoquinol by the cytochrome $b_6 f$ complex = $uN_{PQ_T}N_{cyt_T}$	$\mu mol m^{-2} s^{-1}$
ΔG^0	The Gibbs free energy of activation	J
α	Leaf absorptance in photosynthetically active radiation	NA
β	Fraction of leaf-absorbed energy allocated to PSII	NA
Φ_{PSII}	Photochemical yield of PSII	NA
λ	The outer shell reorganization energy	J
\hbar	The reduced Planck constant	J s

Abbreviations: PQ, plastoquinone; PSII, photosystem II.

We choose to model the states and redox reactions of complexes and electron carriers along the ETC from PSII to Cyt. We represent the feedbacks of the downstream transport from Cyt to PC to PSI to the eventual electron acceptors in the biochemical reactions and photosynthetic controls of electron transport as a boundary condition on the redox dynamics of Cyt. Because of the Cyt's strategic position in the ETC (J. E. Johnson and Berry, 2021; Tikhonov, 2014), applying the boundary condition at Cyt ensures that any feedbacks of downstream processes and biochemical reactions can be summarily represented in the modelling framework. This strategy essentially treats Cyt as the 'control knob' of ETC that is tuned by interacting feedforward and feedback processes of photophysical, photochemical and biochemical reactions.

Once a focus on PSII is decided, the next decision to make is how to represent the various redox states of PSII reaction centres, which determines the overall complexity of the photochemical model. In typical PAM fluorometry, a reaction centre is considered open (O) if the primary quinone acceptor (a tightly bound plastoquinone, Q_A) is in its normal (ground, i.e., oxidized) state and capable of accepting electron for photoreduction whereas a reaction centre is considered closed (C) if Q_A is already reduced and thus unable to accept new electrons and perform photochemistry (Baker, 2008). We use 'OC' to denote this dichotomic representation of PSII reaction centres typical in PAM fluorometry. In modelling studies, the reaction centres can be divided into more redox states. Laisk et al. (2006) represented a PSII reaction centre

with a donor (D) and acceptor (A), which is denoted as the DA representation here. D can be either in the normal (ground, i.e., reduced. D⁰) or oxidized (D⁺) condition and A can be either in the normal (ground, i.e., oxidized, A⁰) or reduced (A⁻) condition. Note that the meaning of the superscript '0' depends on whether the entity is an electron donor or acceptor. The following four redox combinations are possible: D⁰A⁻, D⁰A⁰, D⁺A⁻ and D⁺A⁰. Laisk et al. (2006) considered DOAO and DAO as open reaction centres, and D⁰A⁻ and D⁺A⁻ as closed reaction centres although D⁺A⁰ cannot conduct photochemistry until D⁺ is reduced by the oxygen evolving complex (OEC) and has an electron to be excited by photon energy for donation. Ebenhöh et al. (2011) omitted the D⁺A⁰ state. In contrast, Zhu et al. (2005) and Loriaux et al. (2013) divided the PSII reaction centres based on the redox conditions of QA and the loosely bound plastoquinone (Q_B). We denote this representation as 'QAQB'. QA can be either in the ground state or singly reduced whereas Q_B can be either in the ground state, singly, or doubly reduced state, resulting in six possible redox state combinations. Any combination that has QA in the ground state is considered open; otherwise, it is closed.

In this study, we consider only the OC and Q_AQ_B representations. Using these two contrasting representations allows us to gauge the level of complexity needed to collapse the regulatory mechanisms of electron transport into an informative model for diagnosing, both holistically and atomistically, the ETC performance under the steady state in which electron transport through PSII and PSI is in balance.

Reaction Center

Photosynthetic/ C: Closed PSII ultrastructural **Reaction Center** controls PQH₂ PQ Cyt Ĥ+ O: Open PSII

G-WILEY-

The above representations of PSII reaction centres only concern those that are functionally reversible. Some PSII reaction centres may be inhibited or damaged under stress and thus unable to actively participate in photochemistry (Porcar-Castell, 2011). There are also Q_B-nonreducing PSII reaction centres (Lavergne, 1982). Further, some PSII reaction centres must play a role of cushion because electron transport through PSII occurs in an uneven relay race fashion-the two-electron gate (Stirbet et al., 2020). At the start of the relay, the electron donor can only acquire the energy of one photon and donates one electron at a time. Also, QA can only transfer one electron at a time. Down the chain, however, Q_B must acquire two electrons before picking up two protons from the stroma and joining the free PQ and plastoquinol (PQH₂) pool. This unevenness means that the acceptors of some PSII reaction centres must have already been in a reduced state to provide cushion before any electron transport downstream is possible. In this study, we group the inhibited, Q_B-nonreducing, and cushion PSII reaction centres into an irreversible category which will be represented explicitly in modelling.

FIGURE 2 The movement of electrons through PSII to the cytochrome b₆f complex (Cyt) as represented by the Open (O)-Closed (C) redox reaction model. A functionally active reaction centre can be either in the open state (i.e., the acceptor is in the natural, ground, or re-reduced state) or closed state (i.e., the acceptor is reduced). PQ denotes free plastoquinone whereas PQH₂ denotes plastoquinol. Excitation energy (J_G^*) is needed for the transition from the open to closed PSII state whose back transition is described by the first-order rate constant d. J_G^* is controlled by the light availability and regulated by nonphotochemical quenching (NPQ). r_d and r_r are the second-order rate constants for the electron transfer from the closed reaction centre to plastoquinone to form PQH₂ and for the reverse reaction, respectively. u is the second-order rate constant for the oxidation of PQH2 by the RieskeFeS protein of Cyt and the accompanying transport of proton from the stroma to lumen. The activities of Cyt are regulated by photosynthetic and ultrastructural controls which reflect the feedforward and feedback regulation of electron transport chain and form the boundary condition to close the system of redox equations. [Color figure can be viewed at wileyonlinelibrary.com]

As in Zhu et al. (2005), Laisk et al. (2006), Ebenhöh et al. (2011) and Loriaux et al. (2013), we do not consider the dynamics of the water-splitting reactions by OEC. The dynamics of OEC may constrain J_{PSII} for a given input of excitation energy and other environmental conditions but should not directly affect the steady state photochemical J_{PSII} -q- h_{PQ} - h_{cyt} relationships as we simply ask what q, h_{PQ} and h_{cyt} should be for a given J_{PSII} and vice versa, under the constraints of structural components along the ETC. The same argument is also valid for NPQ which we assume only occurs in lightharvest antenna complexes before the primary charge separation and is not present between the acceptors of PSII and Cvt. NPO controls the allocation of the excitation energy to photochemistry (see Equation 1) but does not directly affect how the allocated photochemical energy is transferred down the ETC in the form of electron and proton fluxes which are governed entirely by the redox poises of relevant protein complexes and carriers. Finally, we do not consider the potential presence of CET and pseudo-CET around PSII. CET and pseudo-CET around PSI have been well established even though the mechanisms controlling these alternative electron flow pathways are still not well understood (Joliot and Johnson, 2011; Nawrocki et al., 2019). Similar alternative pathways may exist for PSII. There have been studies that reported the possibility that not all PQH₂ are oxidized by Cyt, particularly during the dark to light transition (Laisk et al., 2015; Miyake and Okamura, 2003; Saroussi et al., 2019). Electrons of some PQH2 may cycle back to the donor of PSII via a heme in the PSII comlex, cytochrome b₅₅₉, to form the CET of PSII or to oxygen via the plastid terminal oxidase (PTOX) to form pseudo-CET of PSII. Currently, the exact pathways of CET and pseudo-CET of PSII have not been figured out. It is also not clear what physiological functions they may have although they may also involve proton translocation and help protect PSII from photoinhibition as CET and pseudo-CET around PSI do. The equations derived in the following can be updated once future studies have led to a clearer picture about the alternative electron flows around PSII.

Derivation of the OC steady-state photochemical model

Figure 2 depicts the redox reactions and electron movement according to the OC model. The OC model does not distinguish whether the acceptor is primary, secondary, singly, or doubly reduced. The donor of an open reaction centre receives the energy of a photon and donates an electron to its acceptor, closing the reaction centre and initiating the chain of redox reactions. The PQ pool reacts with the pool of closed reaction centres. The model ends at the system boundary with PQH2 being oxidized by Cyt available for LET. The fraction of Cyt available for LET (h_{cvt}) is a dynamic variable to be modelled.

We use O and C to denote the number of reaction centres in the open and closed states, respectively, per unit leaf area (μ mol m⁻²). Major symbols are defined in Table 1. O + C represents the total number of functionally active (reversible) PSII reaction centres. We use I to denote the number of functionally inactive (irreversible) PSII reaction centres per unit leaf area. The following state equations, which can be derived from Figure 2, describe the conversions through redox reactions among the states of PSII and the pools of PQ (denoted by P) and PQH₂ (denoted by H) in the OC model:

3633040, 2023, 5, Downloaded from https://onlinelibrary.wiley.com/doi/10.1111/pce.14563, Wiley Online Library on [29/12/2023]. See the Terms and Conditions (https://onlinelibrary.wiley.com/terms-and-conditions) on Wiley Online Library for rules of use; OA articles are governed by the applicable Creative Commons Licenses.

$$\frac{dO}{dt} = r_d PC - r_r HO - J_G^* + dC = 0.$$
 (2)

$$\frac{dC}{dt} = r_r HO + J_G^* - r_d PC - dC = 0.$$
 (3)

$$\frac{dP}{dt} = \frac{r_r HO - r_d PC}{2} + uN_{cyt_L} H = 0.$$
 (4)

$$\frac{dH}{dt} = \frac{r_d PC - r_r HO}{2} - uN_{cyt_L} H = 0.$$
 (5)

$$O + C + I = N_{PSII}. ag{6}$$

$$P + H = N_{PQT}. (7)$$

Since we are interested in the steady state only, all derivatives with respect to time (t, s) are set to zero, leading to identical pairs of equation between Equations (2) and (3) and between Equations (4) and (5), except for a sign reversion. N_{PSII} and N_{PQT} are the total number of reversible and irreversible PSII reaction centres and the mobile oxidized (P) and reduced (H) plastoquinones per unit of leaf area (μ mol m⁻²), respectively, and assumed to be conserved. N_{cvt_l} is the number of Cyt available (uninhibited) for linear electron transport per unit leaf area and may change with environmental conditions under superimposed photosynthetic and thylakoid ultrastructural controls (details later). J_G^* is the gross rate of charge separation and electron donation from the donor to the acceptor, which is also the rate of conversion from the open to closed reaction action centre (umol m⁻² s⁻¹), and represents the only step of energy input to the ETC. Note that each PSII redox state is changed by one electron (photon) at a time. d is the first-order rate constant for the back transfer of electron from the acceptor to the donor, that is, from the closed to open reaction centre (s⁻¹). r_d and r_r are the second-order rate constant (m² µmol⁻¹ s⁻¹) for the electron transfer from the reduced acceptor to plastoquinone to form PQH₂ and for the reverse reaction, respectively. u is the second-order rate constant ($m^2 \mu$ mol⁻¹ s⁻¹) for the oxidation of PQH₂ by the RieskeFeS protein of Cyt and the accompanying transport of proton from the stroma to the lumen. The factor 2 in the denominator of Equations (4) and (5) accounts for the fact that two electrons are needed to reduce PQ to PQH₂ while the acceptor is only allowed to be singly reduced in the OC model.

Equation (2) shows that

$$r_d PC - r_r HO = J_G^* - dC.$$
 (8)

Combine Equations (4) and (8), and note that two electrons are transported to Cyt for the oxidation of each PQH₂, the electron transport rate out of PSII, J_{PSII} (µmol m⁻² s⁻¹) is therefore

$$J_{PSII} = 2uN_{cyt_L}H = J_G^* - dC.$$
(9)

As expected, J_{PSII} is simply the gross electron flux J_G^* from the donor to the acceptor minus the back transfer. Replace P in Equation (4) by $N_{PQ_T} - H$ and solve for H,

$$H = \frac{r_d C N_{PQ_T}}{r_r O + r_d C + 2u N_{cyt_L}}.$$
 (10)

Insert Equation (10) into (9),

$$J_{PSII} = \frac{2uN_{cyt_{L}}N_{PQ_{T}}r_{d}C}{r_{r}O + r_{d}C + 2uN_{cyt_{L}}}.$$
 (11)

Note that $C = N_{PSII} - I - O$, and the fraction of open PSII reaction centres q is given by $q = \frac{O}{N_{PSII}}$. We use q_r to denote the fraction of the PSII reaction centres that are in the O or C states, that is, the reversible reaction centres.

$$q_r = \frac{O+C}{N_{PSII}}. (12)$$

Equation (11) can then be expressed as

$$J_{PSII} = \frac{2uN_{cyt_{L}}N_{PQ_{T}}(q_{r} - q)}{\left(\frac{r_{r}}{r_{d}} - 1\right)q + \frac{2uN_{cyt_{L}}}{r_{d}N_{PSII}} + q_{r}}.$$
(13)

Equation (13) is not yet an end form of the photochemical J_{PSII} –q relationship because it contains an undetermined variable N_{cyt_L} . If we simply assume Cyt has unlimited potential for oxidizing PQH₂, and N_{cyt_L} does not vary, then Equation (13) is a monotonic function of q. But a monotonic function cannot possibly describe the complex patterns shown in the J_{PSII} –q relationships observed in joint light and CO_2 responses (examples to be given later). To enable modelling nonmonotonic J_{PSII} –q relationships, the dynamic nature of N_{cyt_L} cannot be ignored.

When the demand for electron transport products by the biochemical reactions is limited, the capacity of the RieskeFeS protein and plastocyanin to accept and pass new electrons may be constrained and $N_{\mathrm{cyt}_{\mathrm{L}}}$ may decrease. More generally, we consider four factors that affect N_{cyt_L} . First, the reaction between PQH₂ and the RieskeFeS protein has an optimal lumen pH range of 6.5-7.25 (Foyer et al., 2012). As the lumen pH drops, this reaction becomes slower and can be treated as if N_{cyt_l} decreases. Second, N_{cyt_l} should decrease with increased LET as any Cyt that is being used (reduced) for LET is unavailable for oxidizing new PQH2. Third, CET may compete with LET for Cyt because Cyt catalyzes both LET and CET. This competition may occur if Fd accesses Cyt in grana stacks, rather than Cyt in stroma lamellae, although it may be difficult for the negatively charged Fd to enter stromal gaps as the dimension of Fd is similar to the width of stromal gaps (3~4 nm, Haehnel, 1984; Rantala et al., 2020). CET can be high when environmental conditions arise such that the NADPH/ATP ratio is out of balance and ATP production needs to be boosted to balance this ratio (G. N. Johnson, 2011; Joliot and Johnson, 2011). CET strengthens the proton gradient from the lumen to stroma and contributes to producing ATP but not NADPH. These three factors constitute the photosynthetic controls of ETC (Foyer et al., 2012). Fourth, N_{cyt} may be affected by macromolecular crowding and light-induced thylakoid swelling/shrinking (Kirchhoff, 2014; Kirchhoff et al., 2011; Li et al., 2020). To distinguish from the well-known photosynthetic

controls on electron transport (i.e., those discussed in Foyer et al., 2012), this potential new regulation was termed 'thylakoid ultrastructural control' in the bellows theory that was recently developed to explain the unique thylakoid structure and function of higher plants (Gu et al., 2022). We model the photosynthetic controls together by parsimoniously parameterizing the fraction of Cyt available for LET (h_{cvt}) as a function of q,

$$h_{cyt} = \frac{N_{cyt_L}}{N_{cyt_T}} = f_q \times q = \frac{(1 + a_q)q}{1 + a_q \times q},$$
 (14)

Here N_{cyt_T} is the total number of Cyt per unit leaf area (µmol m⁻²), including both the available (uninhibited) and unavailable (inhibited) complexes for linear electron transport. We italicize the words for linear electron transport to indicate the possibility that N_{cyt_T} in Equation (14) may not necessarily represent the total number of Cyt per unit leaf area for both LET and CET as PSII is mostly located in the grana stacks, PSI in the unstacked stroma lamellae, and Cyt evenly in both domains (Anderson and Anderson, 1980; Danielsson et al., 2004; Koochak et al., 2019; Nevo et al., 2012) and therefore some Cyts may be used exclusively for CET. Thus, h_{cyt} only reflects the redox condition of the Cyt pool that is accessible to LET, that is, the Cyt pool in the grana stacks.

Equation (14) is selected for two primary reasons. First, it has the desired property of $h_{cyt} = 1$ when q = 1, and $h_{cyt} = 0$ when q = 0. In the dark when the ETC is fully relaxed, both h_{cyt} and q should be unity. Conversely, at the hypothetical opposite extreme when all reaction centres are closed (q = 0), all Cyt complexes for LET should be reduced (h_{cvt} = 0) unless plants have some Cyt complexes that can never be used, which would be wasteful and evolutionarily uncompetitive. Equation (14) satisfies both extreme conditions. Second, with a single stoichiometry parameter a_a , Equation (14) permits different possibilities in the redox poise balance between Cyt and PSII. $a_a = 0$ establishes the poise isocline $h_{cyt} = q$; this special case was used in J. E. Johnson and Berry (2021). $a_a > 0$ results in $q_{cvt} > q$, indicating a stronger limitation by PSII on LET compared with Cyt. $a_q < 0$ leads to $h_{cvt} < q$, indicating a stronger limitation by Cyt on LET compared with PSII (Figure 3). Equation (14) combines the effects of photosynthetic controls into a parsimonious and yet flexible function, taking advantage of the fact that these controls do not exist independently of each other, and the electron transport via PSII and PSI is in balance.

For the thylakoid ultrastructural control via thylakoid swelling/shrinking, we develop a representation based on previous electron microscopic studies of thylakoid ultrastructural dynamics and the associated impact on the diffusion of mobile electron carriers within the framework of the bellows theory (Gu et al., 2022). A detailed discussion of this theory is beyond the scope of the present study but a tenet of the theory states that grana stacks of higher plants, acting like bellows in accordions, increase the degree of ultrastructural control on electron transport and photosynthesis through thylakoid swelling/shrinking induced by osmotic water fluxes. The experimental facts that support the thylakoid ultrastructural control and its implication for photosynthetic electron transport and the balance

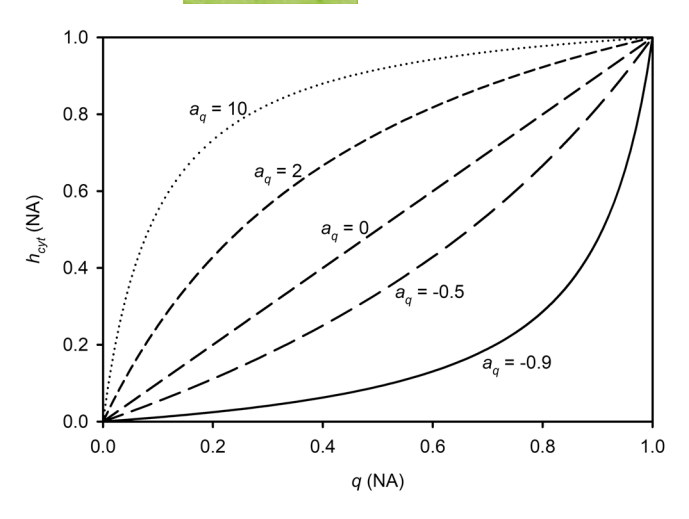


FIGURE 3 The redox stoichiometry relationship between Cyt and PSII. h_{cyt} is the fraction of Cyt available for linear electron transport when the thylakoid is fully expanded. q is the fraction of open PSII reaction centres. The stoichiometry parameter a_q determines how h_{cyt} varies with q. For a given q, h_{cyt} increases with a_q . $a_q = 0$ gives the redox isocline between Cyt and PSII below which Cyt is more strained than PSII and above which Cyt is less strained than PSII for linear electron transport. PSII, photosystem II.

among photophysical, photochemical and biochemical reactions of photosynthesis were discussed thoroughly in the original bellows theory paper (Gu et al., 2022). Here for the purpose of completeness, we summarize the elements of the bellows theory that are directly relevant to the present study.

The volume of thylakoid in higher plants swell in light and shrink in the dark (Kirchhoff, 2014; Kirchhoff et al., 2011; Krause 1973; Murakami and Nobel 1967; Packer et al., 1965). Li et al. (2020) observed an almost doubling of lumen width from 5.0 to 9.4 nm. This magnitude of expansion exceeds the size of PC (~4 nm), which is the mobile electron carrier in the lumen. Lumen swelling is coupled with thylakoid membrane stretching and narrowing of partition gap between widened granal discs. The mechanism of thylakoid swelling requires further investigation but is likely due to the osmotic water fluxes across the thylakoid membrane driven by the disequilibrium in water potential between the lumen and stroma. This disequilibrium develops presumably as the lumen acidifies and ions move across the thylakoid membrane (Beebo et al., 2013; Li et al., 2020). The electron transport from PSII to PSI is coupled with a buildup of transmembrane electric gradient with positivity on the lumen side. This electric gradient leads to ion movement via the ion channels (e.g., passive influx of Cl⁻ or K⁺/H⁺ antiports) in the thylakoid membrane towards the restoration of electroneutrality (Geilfus, 2018; Szabò and Spetea, 2017). Ion fluxes cause disequilibrium in water potential between the lumen and stroma, and therefore osmotic water flow across the thylakoid membrane, which in turn swells the lumen. Ion fluxes also allow the electrical ($\Delta \psi$) and chemical (ΔpH) components of the proton motive force (pmf), which drives the synthesis of ATP, to be flexibly adjusted. This is important because NPQ, which regulates the allocation of excitation energy to photochemistry

3653040, 2023, 5, Downloaded from https://onlinelibrary.wiley.com/doi/10.1111/pce.14563, Wiley Online Library on [29/12/2023]. See the Terms and Conditions (https://onlinelibrary.wiley.com/ecrms-and-conditions) on Wiley Online Library for rules of use; OA articles are governed by the applicable Creative Commons

(Equation 1), depends on ΔpH . An adjustable $\Delta \psi$ to ΔpH ratio facilitates the control of NPQ for photoprotection in response to variations in environmental conditions without the need to change pmf and therefore the synthesis of ATP (Li et al., 2021).

Thylakoid swelling/shrinking affects the diffusion of PQ within the core of lipid bilayer and PC in the lumen, and therefore the electron transport along the ETC. Thylakoid membranes are densely packed with integral protein complexes (e.g., PSII, PSI, Cyt and ATP synthase). These complexes can block the movement of PQ if they sit in its diffusion path. Also, the OEC intrudes deeply into lumen and can hinder the movement of PC. For example, Blackwell et al. (1994) found that the diffusion coefficient of PQ in thylakoids is 100 times slower than that in artificial lipid vesicles free of proteins. The importance of macromolecular blocking for electron transport has been recognized in previous studies (Höhner et al., 2020; Kirchhoff et al., 2011). As the thylakoid swells by the osmotic water influx, macromolecular blocking and the collision probability between carriers and protein complexes and perhaps also between carriers themselves will decrease because the carriers have more room to move around freely in the thylakoid membrane (PQ) or in the lumen (PC), which facilitates the delivery of electrons from PSII to Cyt to PSI. To model the thylakoid ultrastructural control on electron transport, we further modify the h_{cyt} in Equation (14) by a thylakoid swelling/shrinking function f_s to quantify the impact of macromolecular crowding on the diffusion of mobile electron carriers and the availability on Cyt for LET, expressed as

$$f_s = \frac{V}{V_{\text{max}}}.$$
 (15a)

Here V is the volume of the thylakoid at a given set of environmental conditions and V_{max} is the maximum achievable volume of a fully swollen thylakoid. Ideally, dynamic modelling of V/V_{max} should be based on continuous observations of thylakoid volume of a chloroplast in vivo with environmental conditions controlled systematically. Although dark-light contrasts of thylakoid ultrastructure have been observed with electron microscopy (e.g., Li et al., 2020), continuous monitoring of thylakoid ultrastructure of a chloroplast in vivo is currently technologically challenging. Here, we assume, subject to future independent validation, that the swelling of thylakoid resembles, at least to some degree, the swelling of guard cells and vacuoles in the volume-pressure relationship. Of course, the swelling of thylakoid cannot be completely similar to that of guard cells and vacuoles. Chloroplasts do not have a rigid wall to allow a buildup of very high 'turgor' pressure. Although they have a two-membrane envelope, it is not clear whether this envelope plays any role in balancing the osmotic pressure inside the thylakoid. Nevertheless, the difference between the swelling of thylakoid and that of guard cells and vacuoles should be more important at high osmotic pressures when whether there is a rigid wall or not really matters. At low osmotic pressures, assuming some level of resemblance in the volume-pressure relationship between the swelling of thylakoid and that of guard cells and vacuoles should be reasonable. Franks et al. (2001) showed that the relationship between guard cell

volume and turgor pressure appeared to follow a logistic shape. Vitali et al. (2016) modelled the vacuole swelling of *Beta vulgaris* and found that vacuoles expanded logistically to a maximum volume from an initial volume in response to osmotic water inflow. These studies provide hints on how the thylakoid swelling might be modelled. Instead of using many intermediate steps (e.g., environmental conditions \rightarrow pH gradient from lumen to stroma \rightarrow ion fluxes across thylakoid membrane \rightarrow water potential disequilibrium \rightarrow water fluxes into lumen \rightarrow osmotic pressure \rightarrow V) to model the elasticity of thylakoid and the dependency of its swelling on the eventual driving environmental variables, we link V/V_{max} directly to the light intensity via:

$$\frac{V}{V_{\text{max}}} = \frac{1}{1 + c_{\text{e}}e^{-b_{\text{S}}\times\alpha\text{PAR}}}.$$
 (15b)

 f_s is modelled as a sigmoid function of the absorbed photosynthetically active radiation (PAR, μ mol m⁻² s⁻¹) incident upon the leaf with two empirical coefficients b_s and c_s . b_s controls how fast the thylakoid expands and c_s sets the maximum impact of macromolecular crowding on h_{cyt} . f_s equals $1/(1+c_s)$ in the dark and approaches 1 ($V \rightarrow V_{max}$) as PAR increases. Later, we will test the sensitivity of model performance to enabling and disenabling f_s (i.e., setting f_s to 1).

Is it logically acceptable to use a light response function to represent the impact of thylakoid swelling/shrinking on N_{cvti} and therefore on electron transport when light intensity directly affects J_{PSII} and q during the photophysical reactions (see Equation (1) and Figure 1)? Charge separation is the only step along the whole ETC at which photon energy is injected, and all other steps represent energetically downhill reactions on which light intensity has no direct effect. It is true that light intensity directly affects J_{PSII} and qphotophysically. However, how light intensity affects the photochemical relationship between J_{PSII} and q is entirely a different question. All we are asking are the following: for a given value of q, what value should J_{PSII} take? Conversely, for a given value of J_{PSII} , what value should q take? There is no photon receptor that has ever been reported along the ETC between the charge separation steps of PSII and PSI. The answers to these questions only depend on the redox reactions among electron carriers and protein complexes and the diffusion of the carriers in thylakoid membrane and lumen. Thus, if the thylakoid swells continuously as light intensity increases, it is reasonable to assume f_s can capture the impact of this response.

What if the previously observed thylakoid swelling (Kirchhoff, 2014; Kirchhoff et al., 2011; Li et al., 2020) simply represents a switching effect, rather than a dose response of light on thylakoid volume? If this is true, any light intensity would lead to the same degree of thylakoid swelling, and a continuous function such as f_s cannot be used. At the present stage, we cannot rule out this possibility. However, it is hard for us to imagine a possible light-induced mechanism that would switch the volume of thylakoid between two fixed states. It seems the light-induced thylakoid swelling in a dose response due to osmotic water fluxes is a much more parsimonious explanation. Nevertheless, we must emphasize

that the simple function f_s introduced here still requires independent validation against direct observations and should be treated as a starting point, subject to future iterative improvements.

With all four factors considered, N_{cyt_l} is modelled as

$$N_{cyt_L} = N_{cyt_T} f_s f_q \times q.$$
 (16)

So far, we have not explicitly considered the effect of temperature (T, K) on electron transport. To complete the modelling of the photochemical J_{PSII} -q relationship, we assume that redox reactions in thylakoid membrane follow the Marcus theory of electron transfer in proteins, which describes the rate constant of electron transport in proteins (k_{ET}) by (Bostick et al., 2018; Silverstein, 2012)

$$k_{\rm ET} = \frac{2\pi}{\hbar} H_{\rm AD}^2 \frac{1}{\sqrt{4\pi\lambda k_{\rm B}T}} e^{\frac{-(\lambda + \Delta G^0)^2}{4\lambda k_{\rm B}T}}.$$
 (17)

Here ΔG^0 is the Gibbs free energy of activation, λ the outer shell reorganization energy, HAD the quantum mechanical electronic coupling between the initial and final (donor and acceptor) states, $k_{\rm B}$ the Boltzmann constant, and \hbar the reduced Planck constant. We would like to express k_{ET} in terms of its value at a reference temperature ($T_0 = 298.15 \text{ K}$):

$$k_{\text{ETO}} = \frac{2\pi}{\hbar} H_{\text{AD}}^2 \frac{1}{\sqrt{4\pi\lambda k_B T_0}} e^{\frac{-(\lambda + \Delta G^0)^2}{4\lambda k_B T_0}}.$$
 (18)

The standardized temperature response function f_T for the rate constants of redox reactions is given by:

$$f_T = \frac{k_{ET}}{k_{ET0}} = \sqrt{\frac{T_0}{T}} e^{E_T \left(\frac{1}{T_0} - \frac{1}{T}\right)}.$$
 (19)

Here

$$E_T = \frac{(\lambda + \Delta G^0)^2}{4\lambda k_B}.$$
 (20)

 E_{T} is a composite temperature sensitivity parameter (K) related to the Gibbs free energy of activation. $f_T = 1$ for $T = T_0$.

For simplicity, we assume that, when standardized to the same reference temperature, all rate constants of photochemical redox reaction share the same temperature response which cancels in their ratios (e.g., $\frac{r_r}{r_d}$ and $\frac{u}{r_d}$ are temperature-independent even though u, r_d and r_r individually depend on temperature). Thus, in the OC model, temperature affects J_{PSII} via the oxidation rate constant (u) of PQH₂ by Cyt in the nominator of Equation (13), which is not ratioed by another rate constant. Apply f_T only on the u in the nominator and replace N_{cyt_l} in Equation (13) with Equation (16) and we have

$$J_{PSII} = \frac{2uN_{cyt_T}N_{PQT} f_T f_s f_q (q_r - q)q}{\left(\frac{r_r}{r_d} + 2\frac{u}{r_d} \times \frac{N_{cyt_T}}{N_{PSII}} f_s f_q - 1\right)q + q_r}.$$
 (21)

Note that the rate constants u, r_d and r_r in Equation (21) should now be understood as denoting their values at T_0 and are invariant constants.

Equation (21) can be used to fit measurements of J_{PSII} and qmade with PAM fluorometry to estimate redox parameters at the leaf level. It is important to point out that, in such fitting, $uN_{cyt_T}N_{PQ_T}$, $\frac{r_r}{r_d}$ and $\frac{u}{r_d} \times \frac{N_{cyt_T}}{N_{pSII}}$ should be treated as if they are single parameters as their components cannot be individually resolved. We call them composite parameters and for the sake of simplification, denote them respectively by,

$$U = uN_{cyt_T}N_{PQ_T}. (22)$$

$$R_1 = \frac{r_r}{r_d}. (23)$$

$$R_2 = \frac{u}{r_d} \times \frac{N_{cyt_T}}{N_{PSU}}.$$
 (24)

Using these notations, Equation (21) is expressed as

$$J_{PSII} = \frac{2Uf_T f_s f_q (q_r - q)q}{(R_1 + 2R_2 f_s f_q - 1)q + q_r}.$$
 (25)

U represents the maximum oxidation potential of the PQ + PQH₂ pool by Cyt. R₁ and R₂ are interpreted as the first and second resistance of electron transport of PSII, respectively. The independent parameters in Equation (25) are the composite parameters U (μ mol m⁻² s⁻¹), R_1 (unitless), and R_2 (unitless) and single parameters q_r (unitless), a_q (unitless) in the function f_q , b_s (µmol⁻¹ m² s) and c_s (unitless) in the function f_s , and E_T (K) in the function f_T . Whether all these parameters can be estimated by fitting Equation (25) into measurements depends on the nature of the measurements. For example, if the data contain only CO₂ response where light is held at a constant level, b_s and c_s cannot be estimated and must be given a value a priori or f_s must be set to 1. For measurements where temperature is held at a constant level, E_T must be given a value a priori or f_T should be set to 1.

At this point, let us compare Equation (1) with Equation (25). We see that NPQ appears in Equation (1) but not in Equation (25). Why? This is because different dissipation pathways, including NPQ, compete for the excitation energy before it reaches the reaction centres. The outcome of this competition for photochemistry is described by Equation (1). In contrast, Equation (25) describes what happens after the excitation energy has been delivered to the reaction centres, and NPQ, which quenches excitation energy/ fluorescence and is not a process for diverting electrons, does not play direct roles in events occurring post PSII. For the same reason, PAR is the source of energy in Equation (1) but in Equation (25), it acts only as a predictor for the thylakoid swelling/shrinking

To facilitate the inference of the redox state of the free plastoquinone pool from leaf PAM fluorometry measurements, we derive an expression for the fraction of the PQ + PQH₂ pool that is oxidized (h_{PO} , i.e., in PQ). Use Equations (7) and (10),

$$h_{PQ} = \frac{P}{N_{PQT}} = 1 - \frac{H}{N_{PQT}} = \frac{r_r O + 2u N_{cyt_L}}{r_r O + r_d C + 2u N_{cyt_L}}.$$
 (26)

3633040, 2023, 5, Downloaded from https://onlinelibrary.wiley.com/doi/10.1111/pce.14563, Wiley Online Library on [29/12/2023]. See the Terms and Conditions (https://onlinelibrary.wiley.com/terms-and-conditions) on Wiley Online Library for rules of use; OA articles are governed by the applicable Creative Commons. License, and Conditions (https://onlinelibrary.wiley.com/terms-and-conditions) on Wiley Online Library for rules of use; OA articles are governed by the applicable Creative Commons. License, and Conditions (https://onlinelibrary.wiley.com/terms-and-conditions) on Wiley Online Library for rules of use; OA articles are governed by the applicable Creative Commons. License, and Conditions (https://onlinelibrary.wiley.com/terms-and-conditions) on Wiley Online Library for rules of use; OA articles are governed by the applicable Creative Commons. License, and Conditions (https://onlinelibrary.wiley.com/terms-and-conditions) on Wiley Online Library for rules of use; OA articles are governed by the applicable Creative Commons. License, and Conditions (https://onlinelibrary.wiley.com/terms-and-conditions) on Wiley Online Library for rules of use; OA articles are governed by the applicable Creative Commons. License, and the conditions (https://onlinelibrary.wiley.com/terms-and-conditions) on Wiley Online Library for rules of use; OA articles are governed by the applicable Creative Commons.

With $C = N_{PSII} - I - O$, $q = \frac{O}{N_{PSII}}$ and $q_r = 1 - \frac{I}{N_{PSII}}$, we divide the nominator and denominator of Equation (26) by $r_d N_{PSII}$ to transform it into:

$$h_{PQ} = \frac{\frac{r_r}{r_d} q + 2\frac{u}{r_d} \times \frac{N_{Cyt_L}}{N_{PSII}}}{\left(\frac{r_r}{r_d} - 1\right) q + q_r + 2\frac{u}{r_d} \times \frac{N_{Cyt_L}}{N_{DSII}}}.$$
 (27)

Insert Equation (16) into Equation (27) and notice Equations (23) and (24), we have

$$h_{PQ} = \frac{R_1 + 2R_2 f_s f_q}{(R_1 + 2R_2 f_s f_q - 1)q + q_r} q.$$
 (28a)

Alternatively, we can express the fraction of the PQ + PQH₂ pool that is reduced (h_{POH_2} , i.e., in PQH₂).

$$h_{PQH_2} = 1 - q_{PQ} = \frac{q_r - q}{(R_1 + 2R_2 f_s f_a - 1)q + q_r}.$$
 (28b)

The redox states of the free plastoquinone pool (h_{PQ} or h_{PQH_2}) and Cyt for LET (h_{cyt}) can now be estimated with Equations (28) and (14), respectively, by fitting Equation (25) into PAM fluorometry measurements for relevant leaf redox parameters.

2.3 | Derivation of the Q_AQ_B steady-state photochemical model

Figure 4 describes the redox reactions and electron movement according to the Q_AQ_B model. The state equations and the derivation of the corresponding steady-state photochemical model are given in the Supporting Information: 1 in the Appendices. The steady-state $J_{PSII}-q$ relationship is obtained by solving the following cubic equation:

$$J_{PSII}^3 + a_2 J_{PSII}^2 + a_1 J_{PSII} + a_0 = 0. {(29)}$$

Here,

$$(2R_{2}f_{s}f_{q}-k_{2})(R_{1}+2R_{2}f_{s}f_{q})q+\frac{2Uf_{s}f_{q}(R_{1}-1-k_{AB})}{k_{PSII}}q + \left[\frac{2Uf_{s}f_{q}(1+k_{AB})}{k_{PSII}}q+k_{1}R_{1}q-k_{1}q-2q+2q_{r}\right]$$

$$a_{2}=\frac{(R_{1}+2R_{2}f_{s}f_{q}-1)}{(R_{1}+2R_{2}f_{s}f_{q}-1)(R_{1}-1-k_{AB})/(k_{PSII}f_{r})}.$$
(30)

$$a_{1} = \frac{\left(k_{1}R_{1} + k_{2}R_{1} + 2k_{2}R_{2}f_{s}f_{q} + \frac{2Uf_{s}f_{q}(1 + k_{AB})}{k_{PSII}}\right)q^{2}}{(R_{1} + 2R_{2}f_{s}f_{q} - 2)q}$$

$$a_{1} = \frac{+(k_{1}q + 2q - 2q_{r})(R_{1} + 2R_{2}f_{s}f_{q} - 2)q}{(R_{1} + 2R_{2}f_{s}f_{q} - 1)(R_{1} - 1 - k_{AB})/\left(2Uf_{1}^{2}f_{s}f_{q}k_{PSII}\right)}.$$
(31)

$$a_0 = \frac{4U^2 f_T^3 f_s^2 f_q^2 k_{PSII} (k_1 q + 2q - 2q_r) q^2}{(R_1 + 2R_2 f_s f_q - 1)(R_1 - 1 - k_{AB})}.$$
 (32)

The Q_AQ_B model has four new parameters in addition to those that appear in the OC model. They are k_1 , k_2 , k_{AB} and k_{PSII} .

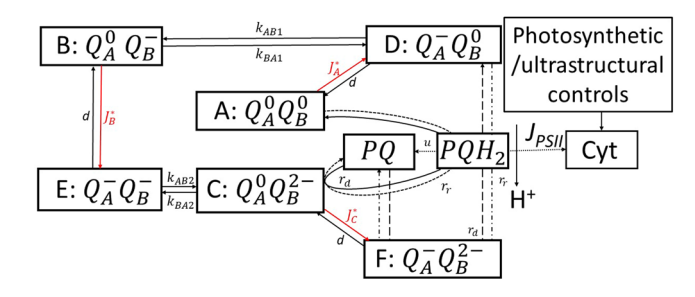


FIGURE 4 The movement of electrons through PSII to the cytochrome b₆f complex (Cyt) as represented by the Q_AQ_B redox reaction model. The tightly-bound plastoquinone (Q_A) can be either in the ground state (Q_A^0) or reduced state (Q_A^-) whereas the looselybound plastoquinone (Q_B) can be either in the ground state (Q_B^0), singly reduced state (Q_B^-) , or doubly reduced state (Q_B^{2-}) . The resultant six PSII states are denoted by A, B, C, D, E and F, respectively. Excitation energy is consumed in three scenarios when Q_A accepts an electron and changes the redox state from Q_A^0 to $Q_A^$ as indicated by J_A^* , J_B^* and J_C^* , respectively. The gross excitation energy flux $J_G^* = J_A^* + J_B^* + J_C^*$ is controlled by the light availability and regulated by nonphotochemical quenching (NPQ). k_{AB1} and k_{AB2} are the first-order rate constant for the transfer of electron from the reduced Q_A to the ground and singly reduced Q_B to form the states of $Q_A Q_B^-$ and $Q_A Q_B^{2-}$, respectively while k_{BA1} and k_{BA2} are the firstorder rate constants for the corresponding reverse transfer of electron. r_d and r_r are the second-order rate constant for the electron transfer from Q_B²⁻ to PQH₂ and for the reverse reaction, respectively. u is the second-order rate constant for the oxidation of PQH₂ by the RieskeFeS protein of Cyt and the accompanying transport of proton from the stroma to lumen. While the same labels u, r_d and r_r are used in the OC and Q_AQ_B model, they may have different values in the two models because the reactants are different. The activities of Cyt are regulated by photosynthetic and ultrastructural controls which reflect the feedforward and feedback regulation of electron transport chain and form the boundary condition to close the system of redox equations. PSII, photosystem II. [Color figure can be viewed at wileyonlinelibrary.com]

 $k_1 = \frac{k_{BA1}}{k_{AB1}}$, $k_2 = \frac{k_{BA2}}{k_{AB2}}$, $k_{AB} = \frac{k_{AB1}}{k_{AB2}}$, $k_{PSII} = k_{AB1}N_{PSII}$. k_{AB1} and k_{AB2} are the first-order rate constant (s⁻¹) for the transfer of electron from the reduced Q_A to the ground and singly reduced Q_B to form the states of $Q_A Q_B^-$ and $Q_A Q_B^2^-$, respectively while k_{BA1} and k_{BA2} are the first-order rate constant (s⁻¹) for the corresponding reverse transfer of electron (Figure 4). The same f_T , f_q and f_s apply to the $Q_A Q_B$ model as in the OC model. Similarly, only un-ratioed rate constants are subject to temperature modification.

Under the Q_AQ_B model, h_{cyt} is still calculated with Equation 14 but h_{PQ} is given by (Supporting Information: 1):

$$h_{PQ} = 1 - \frac{J_{PSII}}{2Uf_T f_S f_a \times q}$$
 (33a)

Or,

$$h_{PQH_2} = \frac{J_{PSII}}{2Uf_T f_S f_a \times q}.$$
 (33b)

3 | C₃/C₄ DATA SETS FOR TESTING THE STEADY-STATE PHOTOCHEMICAL MODELS

We use a data set collected by the Leafweb project (www.leafweb. org) to evaluate the derived OC and QAQB models. This data set, which is fully documented in the data citation Han, Zhang, et al. (2022), contains measurements of PAM fluorometry of light, CO₂, O₂ and temperature responses from 23 C₃ and four C₄ species in Canada, China, Finland, The Netherlands and USA. For completeness, key details about the measurement methods and protocols are also described in Supporting Information: 2 Materials and Methods. The species include three lianas, three shrubs, two boreal deciduous trees, one boreal evergreen needle-leaf tree, three temperate deciduous trees, four tropical deciduous trees, three tropical evergreen trees, one C₃ grass, three C₄ grasses and five crop varieties. Supporting Information: Table S1 lists the species, locations, data types, and sources. The data set consists of both previously used and new data from multiple investigators using standard PAM fluorometry (Baker, 2008) and gas exchange (Long and Bernacchi, 2003) measurement protocols. The data from Scots pine contain 1-year continuous fluorometry observations made at intervals of 10 or 30 min in the field under natural environments using Walz monitoring PAM (Porcar-Castell, 2011). Measurements from all other 26 species include simultaneous PAM fluorometry and gas exchange observations. However, the measured net assimilation rates of leaf photosynthesis are not used in the present study. Among these 26 species, 7 species were measured with light response curves only (i.e., light intensity varied systematically with ambient CO2 concentration controlled at a constant level, e.g., 400 ppm). All the other 19 species were measured with both the light response and CO₂ response (i.e., ambient CO₂ concentration varied systematically with light intensity controlled at a constant level, e.g., 2000 µmol m⁻²s⁻¹). For most species, measurements were made with temperature controlled at ~25°C with the exceptions of Scots pine (natural diurnal and seasonal variations), tomato cultivar Basket Vee (~21°C), and cotton which contained temperature stress experiments (9°C to 40°C). All measurements were made at ambient O2 concentration except for the tomato cultivar Basket Vee and cotton which used two O2 levels (2% and 21%) and rice and tomato cultivar Growdena which used five O2 levels (2%, 10%, 21%, 35% and 50%).

All PAM fluorometry measurements started with fully darkadapted leaves to determine the minimum (F_0) and maximum (F_M) fluorescence yield. The exception is the case of Scots pine for which a monitoring PAM was used and the point in the time series where the maximum fluorescence yield peaked in night (typically before sunrise) was treated as F_M and the corresponding steady state fluorescence yield was treated as F_0 (because there was no light in night). The F_M and Fo obtained in this way were used as dark-adapted measurements for the following day (Porcar-Castell, 2011). The photochemical quantum yield of PSII (Φ_{PSII}) was calculated as $1 - \frac{F_S}{FL}$ as in standard fluorometry (Genty et al., 1989) where F_s is the steady state fluorescence yield in the daytime or with the actinic light on and F'_{M} is

the corresponding maximum fluorescence yield obtained with a saturation pulse. J_{PSII} is calculated with $J_{PSII} = \Phi_{PSII} \times \alpha\beta PAR$. $\alpha = 0.85$ is the leaf absorptance in PAR, and β = 0.5 is the fraction of absorbed PAR allocated to PSII. q is calculated either as the fraction of open PSII reaction centres with the lake connectivity of photosynthetic units (q_1) or as that with the puddle connectivity (q_P) (Kramer et al., 2004). F'_0 , which is the minimum fluorescence yield with all PSII reaction centres open but NPQ unrelaxed and needed for the calculation of q_L and q_P , is calculated with the Oxborough-Baker approach (Oxborough and Baker, 1997). Only q₁-based results are reported in this study because the two redox models work equally well for the J_{PSII} - q_L and J_{PSII} - q_P relationships and no conclusion needs to be modified when q_P is used.

PERFORMANCE OF THE STEADY-STATE PHOTOCHEMICAL MODELS

We fitted the steady-state photochemical models to the datasets collected to evaluate their performance. A hybrid global optimization algorithm that applies evolutionary method, gradient descent, and compass search in sequence with repeated random guess reinitialization was used in the fitting. This algorithm is described in Supporting Information: Photochemical parameter estimation methods. To facilitate the applications of the OC model by researchers, we have developed an Excel Spreadsheet tool that implements the evolutionary method. Supporting Information: An Excel spreadsheet tool for optimizing the open-closed (OC) redox model of photosynthetic electron transport provides instructions on how to use this tool.

We first validated the derived OC and QAQB models with the leave-one-out cross-validation approach (Vehtari et al., 2017). To do so, the measurements of each sample were evenly divided into an optimization data group and a validation data group. The optimization data group was used to fit the OC and Q_AQ_B models, and the validation data group was used to validate the models with the optimized parameters from the optimization data group. The OC model performed almost equally well for the optimization (Supporting Information: Figure S1a) and validation (Supporting Information: Figure S1c) data groups ($r^2 > 0.98$, slope~0.99, and p < 0.01). The Q_AQ_B model performs marginally better than the OC model for the optimization data group (compare Supporting Information: Figure S1b vs. S1a). For the validation data group, however, the Q_AQ_B model predicted some values of J_{PSII} that were unreasonably large (Supporting Information: Figure S1d), indicating the optimized parameters from the optimization data group may not be reliable for this model. The QAQB model is more complex and has four more independent parameters. Since it performed only marginally better than the simpler OC model, it may have redundant parameters whose optimized values may be affected by overfitting and not represent physiological reality for a given set of measurements. We consider the OC model passed the test of model validation while the application of the QAQB model requires precaution due to potential

3633040, 2023, 5, Downloaded from https://onlinelibrary.wiley.com/doi/10.1111/pce.14563, Wiley Online Library on [29/12/2023]. See the Terms and Conditions (https://onlinelibrary.wiley.com/terms-and-conditions) on Wiley Online Library for rules of use; OA articles are governed by the applicable Creative Commons. License, and Conditions (https://onlinelibrary.wiley.com/terms-and-conditions) on Wiley Online Library for rules of use; OA articles are governed by the applicable Creative Commons. License, and Conditions (https://onlinelibrary.wiley.com/terms-and-conditions) on Wiley Online Library for rules of use; OA articles are governed by the applicable Creative Commons. License, and Conditions (https://onlinelibrary.wiley.com/terms-and-conditions) on Wiley Online Library for rules of use; OA articles are governed by the applicable Creative Commons. License, and Conditions (https://onlinelibrary.wiley.com/terms-and-conditions) on Wiley Online Library for rules of use; OA articles are governed by the applicable Creative Commons. License, and Conditions (https://onlinelibrary.wiley.com/terms-and-conditions) on Wiley Online Library for rules of use; OA articles are governed by the applicable Creative Commons. License, and the conditions (https://onlinelibrary.wiley.com/terms-and-conditions) on Wiley Online Library for rules of use; OA articles are governed by the applicable Creative Commons.

parameter overfitting. In the following, we pooled the data and refitted the models. The results reported below were from the pooled data.

As shown in Figure 5, the J_{PSII} –q relationship is nonmonotonic because J_{PSII} can either increase or decrease with q, depending on how such changes are induced and whether the carboxylation in the downstream carbon reactions is limited by RuBP regeneration (i.e., light, or electron transport rate) or by Rubisco (CO₂ supply). In typical light response measurements where ambient CO₂ concentration is held constant and carboxylation is limited by RuBP regeneration, J_{PSII} increases but q decreases as light intensity

gradually increases and more acceptors of PSII are necessarily reduced (the right side in each plot of Figure 5). At saturating light intensities, however, J_{PSII} and q may decrease simultaneously as too many reaction centres are closed and CO_2 supply (Rubisco) limits carboxylation (the left end of the curves in Figure 5a-c,i). In typical CO_2 response measurements where light intensity is held constant and carboxylation is limited by Rubisco, increased CO_2 concentration will increase the demand for electron transport products and help drain the accumulated electrons from the reduced acceptors of PSII faster and thus both J_{PSII} and q will increase simultaneously (the left side in Figure 5d-h). Additional

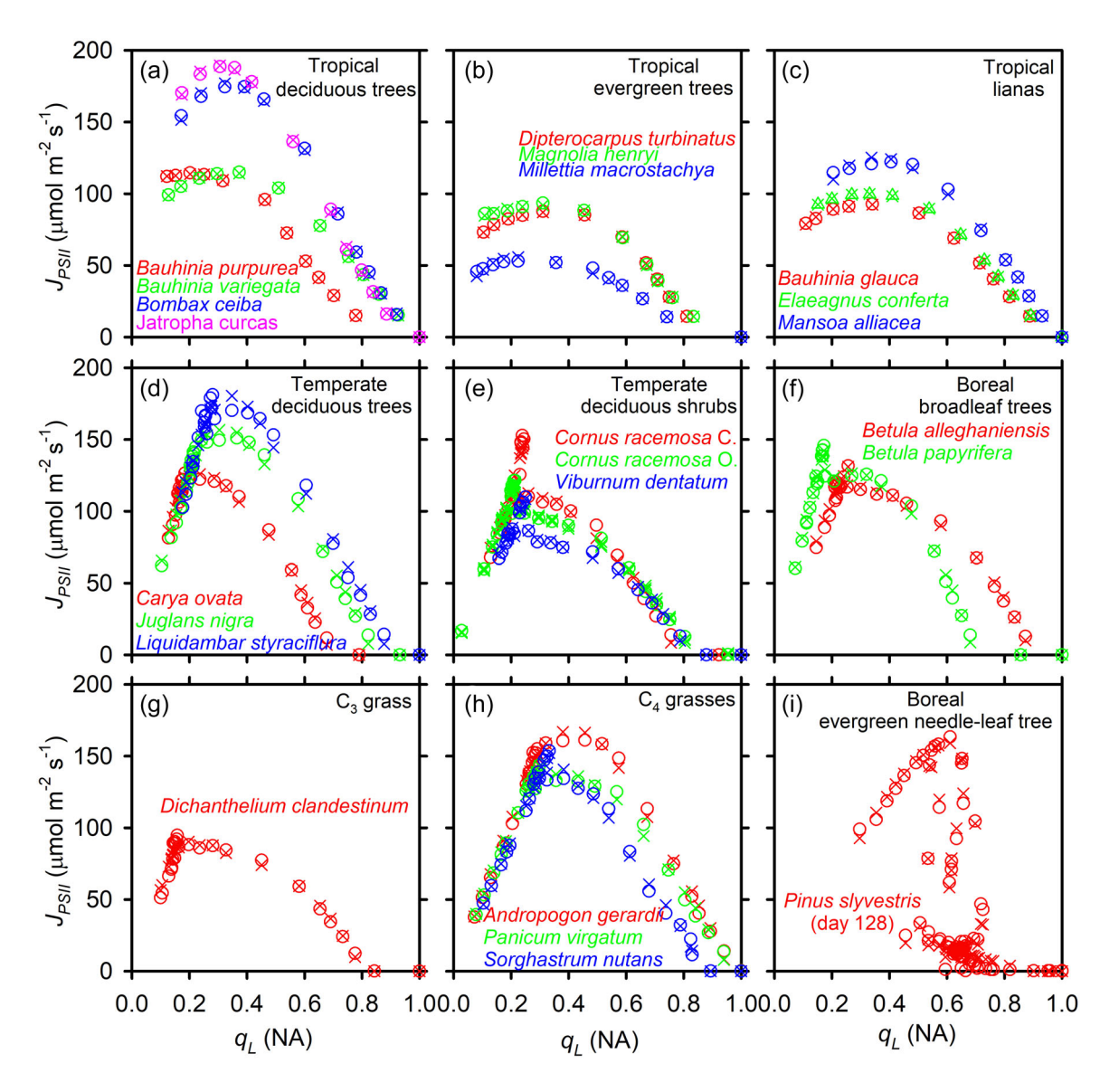


FIGURE 5 Examples demonstrating the performance of the OC model for predicting the linear electron transport rate (J_{PSII}) as a function of fraction of open PSII reaction centres (q_L) with the lake connectivity of photosynthetic units for a variety of noncrop species. The thylakoid swelling is enabled. Measurements are either from light response only—systematic variation of light intensity at a fixed ambient CO_2 concentration (a, b and c), or light response in conjunction with CO_2 response—systematic variation of ambient CO_2 concentration at a fixed light intensity (d, e, f, g and h), or natural diurnal environmental variations (i). J_{PSII} and q generally vary in the opposite direction for light response but in the same direction for CO_2 response. Colours, circles, and × denote species, measurements, and model fits, respectively. All model fits have $r^2 > 0.97$ and p < 0.001.

13653040, 2023, 5, Downloaded from https://onlinelibrary.wiley.com/doi/10.1111/pce.14563, Wiley Online Library on [29/12/2023]. See the Terms and Conditions (https://onlinelibrary.wiley.com/erm

and-conditions) on Wiley Online Library for rules of use; OA articles are governed by the applicable Creative Commons License

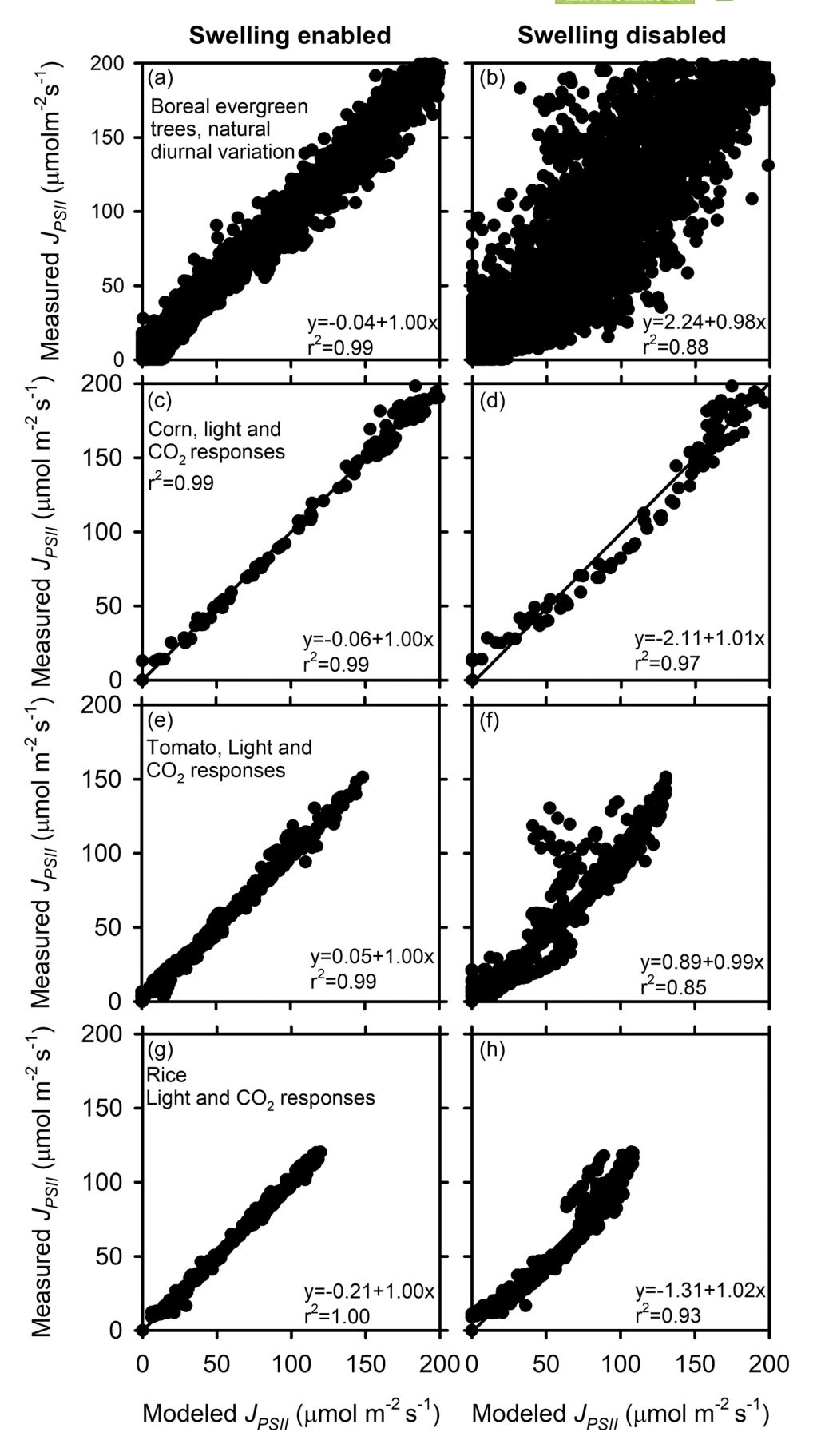


FIGURE 6 A comparison of the OC-modelled versus measured linear electron transport rate (J_{PSII}) for species of boreal evergreen trees (a and b), corn (c and d), tomato (e and f) and rice (g and h) with the thylakoid swelling either enabled (the left column) or disabled (the right column). Line indicates linear regression. All regressions are significant at p = 0.01.

3653040, 2023, 5, Downloaded from https://onlinelibrary.wiley.com/doi/10.1111/pce.14563, Wiley Online Library on [29/12/2023]. See the Terms and Conditions (https://onlinelibrary.wiley.com/term

-conditions) on Wiley Online Library for rules of use; OA articles are governed by the applicable Creative Commons License

examples of the similar nonmonotonic patterns described above are found in Supporting Information: Figure S2. Both the OC model (Figure 5 and Supporting Information: Figure S2) and the Q_AQ_B model (Supporting Information: Figures S3 and S4) fit these general patterns accurately.

When the thylakoid swelling/shrinking function f_s is enabled, both the OC and Q_AQ_B models produce tight fits $(r^2 \approx 1)$ of the J_{PSII} -q relationship in our data sets (for OC, Figure 5, the left panels

of Figures 6 and 7, Supporting Information: Figure S2, and the left panels of Supporting Information: Figures S5–S7; for Q_AQ_B , Supporting Information: Figures S3 and S4, the left panels of Supporting Information: Figures S8–S12). There are a few visible outliers in comparisons of the OC-modelled versus measured J_{PSII} , for example, near the origins of Supporting Information: Figures S6a, S6c and S7c. These outliers disappear in the corresponding comparisons of the Q_AQ_B -modelled versus

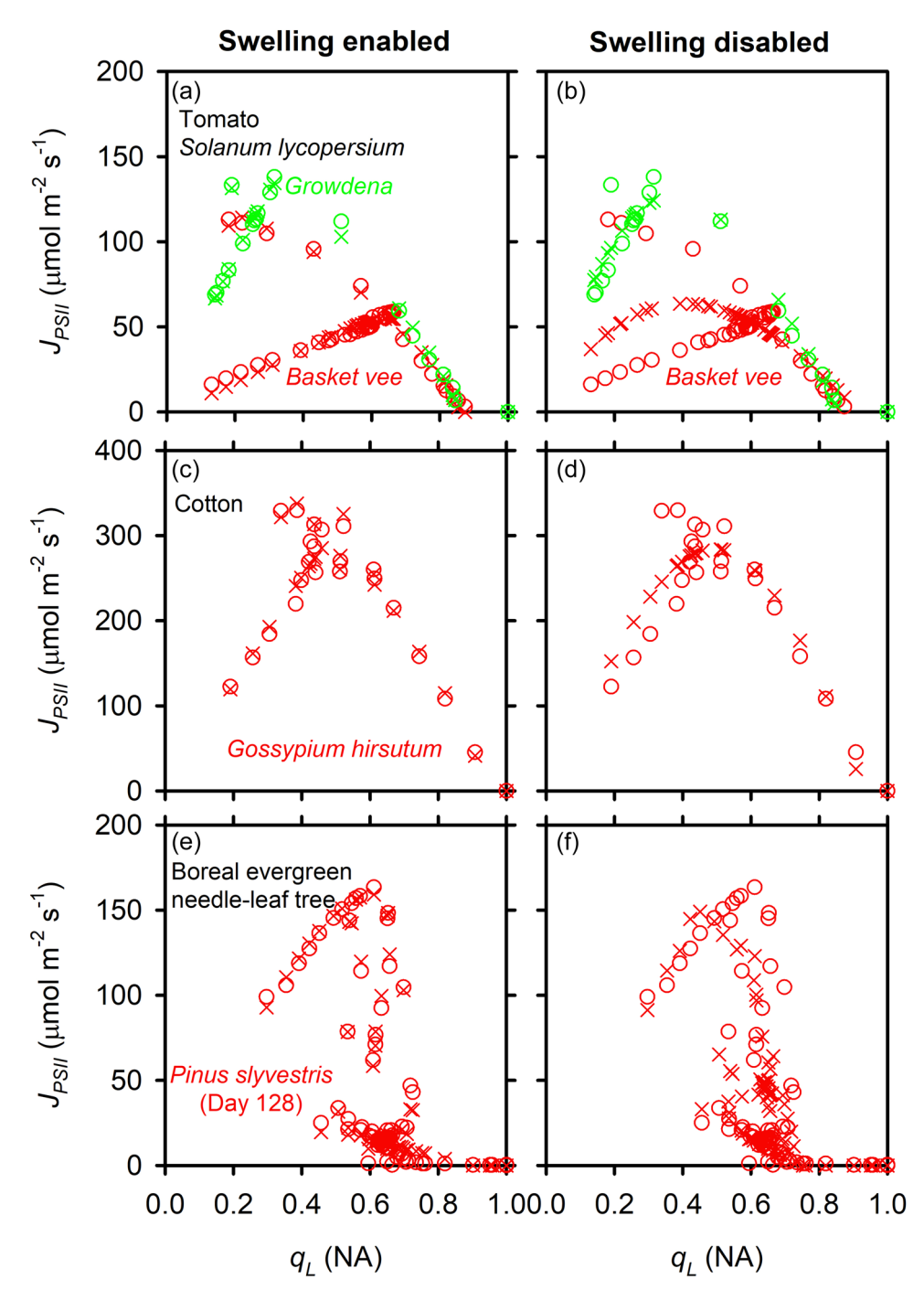


FIGURE 7 Examples demonstrating the performance difference of the OC model for predicting the linear electron transport rate (J_{PSII}) as a function of fraction of open PSII reaction centres (q_L) with the lake connectivity of photosynthetic units with the thylakoid swelling enabled (left column) or disabled (right column).

3653040, 2023, 5, Downloaded from https://onlinelibrary.wiley.com/doi/10.1111/pce.14563, Wiley Online Library on [29/12/2023]. See the Terms and Conditions (https://onlinelibrary.wiley.com/term

and-conditions) on Wiley Online Library for rules of use; OA articles are governed by the applicable Creative Commons License

measured J_{PSII} (Supporting Information: Figure S9a, 9c and S11c). These out-of-pattern points are due to some unusually large measured J_{PSII} when all PSII reaction centres approach full opening at low light intensities, which indicates the measured F'_m and/or F_s of these points may be at error. Thus, the apparent tight fitting of these points by the more complex QAQB model may indicate overfitting, rather than a deficiency of the OC model. This is consistent with our assessment of the QAQB model obtained during model validation. The broad applicability and high performance of the redox models, particularly the simpler OC model, support our novel representations of the photosynthetic and thylakoid ultrastructural controls on electron transport.

When the ultrastructural control is disabled by forcing $f_s = 1$, we observed significant drop in the performance of the OC and QAQB models to fit the observed J_{PSII} -q relationship for all species, which is illustrated by comparing the left and right panels of Figures 6 and 7, and Supporting Information: S5-S12. Across species, disabling the ultrastructural control reduces r^2 and increases the root mean square error and the corrected Akaike information criterion (AIC_c) of the fitting (Supporting Information: Table S2). The increase in AIC. indicates that the drop in the performance of the OC and Q_AQ_B models when the ultrastructural control is not represented is not due to a reduced number of tunable parameters but due to a lack of adequate process representation. The drop in model performance is

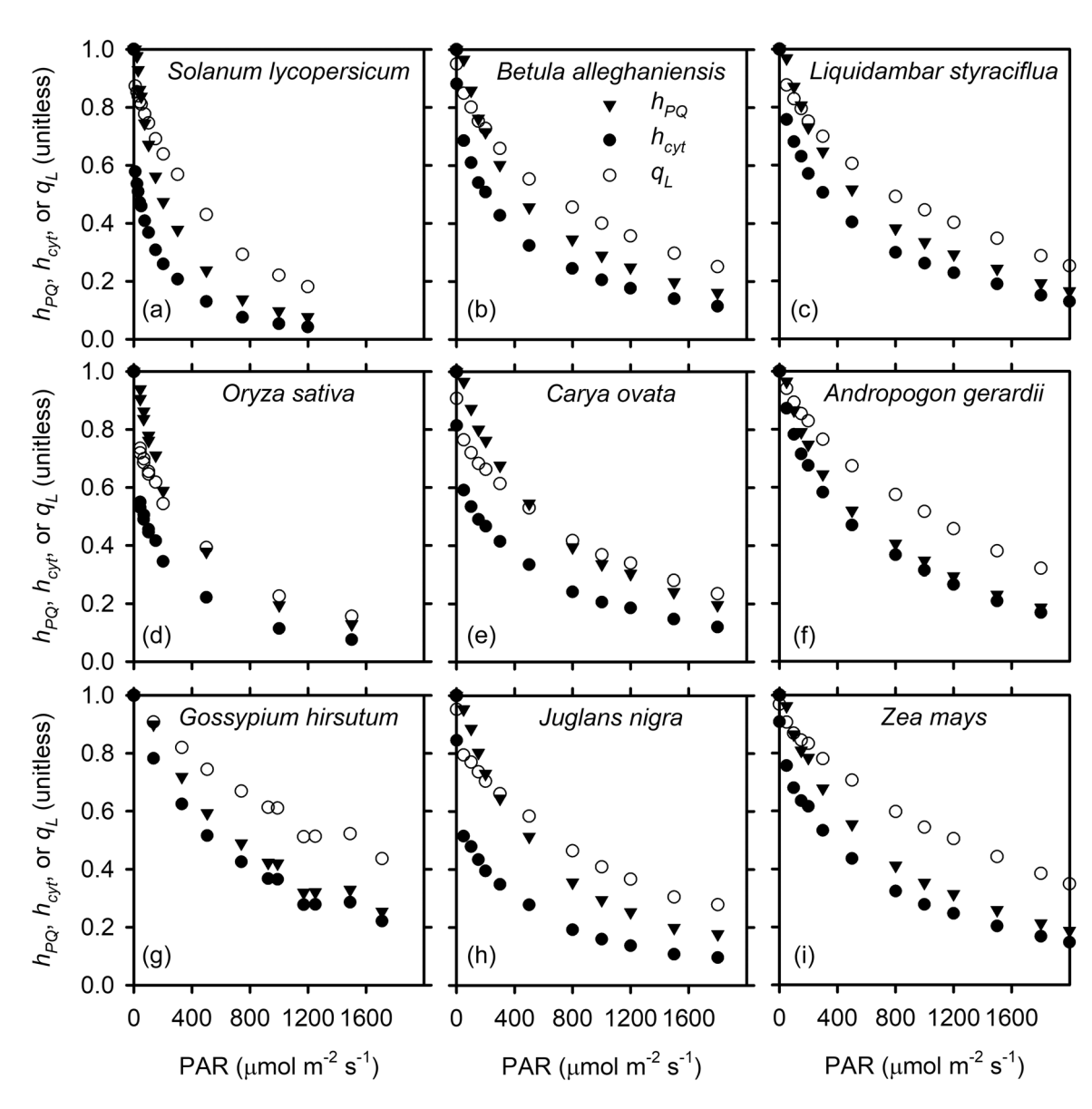


FIGURE 8 Examples of the change in the oxidized fraction of mobile plastoquinone pool (h_{PO}, triangle), the fraction of cytochrome b₆f complex available for linear electron transport (h_{cyt} , solid dot), and the fraction of open photosystem II reaction centres under the assumption of lake model $(q_L, \text{ circle})$ as a function of photosynthetically active radiation (PAR). Each plot is for a different species. See Supporting Information: Table S1 for general measurement conditions for these species. h_{PQ} and h_{cyt} are obtained with the OC model whose parameters are given in Supporting Information: Table S3.

worse for samples where light and CO2 responses are jointly measured but CO₂ responses are measured at sub-saturating rather than saturating light levels (Figure 7a-d, Supporting Information: Figure S12a-d) or when measurements represent natural diurnal variations (Figure 7e,f, Supporting Information: Figure S12e,f). The reason for this performance difference is that at saturating light intensity, the thylakoid is fully swollen, and f_s is close to unity and thus plays little role in the fitting. Our findings suggest that without representing the ultrastructural control, the redox models cannot simultaneously describe the relationships between the electron transport rate and redox state of PSII reaction centres under low and high light conditions. These results suggest that representing the thylakoid ultrastructural control, which in the present modelling framework is rather simplistic, appears to be an essential requirement for modelling LET in response to variations in environmental conditions.

The inferred h_{PQ} and h_{cyt} decrease with increasing light intensity as the measured q_L does across species (Figure 8, which was produced with the OC model whose parameter values are given in Supporting Information: Table S3). However, they do not follow the same trajectory. The differences between h_{PQ} , h_{cyt} and q_L mean that the redox status of PSII, which can be directly monitored with PAM fluorometry, does not necessarily indicate the redox status of the mobile plastoquinone or Cyt pools. For the same light level, h_{cvt} is generally less than h_{PO} and q_L across species, indicating that Cyt is the bottleneck of the electron transport chain. Support for Cyt being a bottleneck also comes from the optimized value of $R_2 = \frac{u}{r_d} \times \frac{N_{cyt_T}}{N_{PSII}}$. For most cases, the optimized R_2 is less than 0.0001 (Supporting Information: Table S3), which indicates $u \times N_{cyt_T}$ is much less than $r_d \times N_{PSII}$, that is, the capacity of PQH₂ oxidation by Cyt is much smaller than the capacity of PQ reduction by the reduced PSII acceptor across species (Figure 2).

5 | DISCUSSIONS AND CONCLUSIONS

An immediate insight from the theoretical derivation and leaf-level validation of the overall photochemical J_{PSII} -q relationship is that while numerous free redox parameters and protein complex/electron carrier concentrations affect the dynamics of the ETC, which reflects the complexity of its structure and regulation, a high degree of redundancy exists in the functions they have. All redox rate constants and protein complex/electron carrier concentrations occur in products and ratios. As a result, changes in one parameter can be directly compensated for by changes in other parameters. Consequently, values of individual parameters such as redox reaction rate constants and foliar concentrations of reaction centres, mobile plastoquinone, and Cyt cannot be resolved with leaf-level measurements alone. Fortunately, complex photochemical processes are described by a few truly independent composite parameters that control the photochemical J_{PSII} -q relationships and can be inferred from the commonly available PAM fluorometry

measurements at the leaf level. The OC model is more parsimonious and fully consistent with the open-closed dichotomy of PSII reaction centre representation in PAM fluorometry, and its independent parameters can be better constrained by leaf-level measurements as compared to the Q_AQ_B model. Since these two models perform almost equally well, we recommend the OC model for general applications.

Although only composite parameters (e.g., U, R_1 and R_2) can be inferred at the leaf level with our model and PAM fluorometry measurements, individual parameters (e.g., u, r_d and r_r) can be calculated from the estimated composite parameters if N_{PSII} , N_{PQ_T} , and N_{cyt_T} are known (see Equations 22–24). Development of measurement techniques for assaying N_{PSII} , N_{PQ_T} , and N_{cyt_T} after PAM fluorometry measurements are conducted will greatly advance the research in photosynthetic electron transport in natural environments. Since the composite parameters define the efficiency of the photosynthetic electron transport chain, it would be interesting to investigate how they vary with species, climate, nutrient availability and mineral deficiencies (Ohnishi et al., 2021).

Ideally, the photochemical model developed in this study should be tested at multiple hierarchies. At the lowest hierarchy, if the redox states of the PQ pool and Cyt could be monitored directly and quantified, then such measurements can be compared with the predicted redox states of PQ and Cyt (i.e., h_{PO} and h_{cvt}). At the intermediate hierarchy, although the light-induced thylakoid swelling/shrinking is a well-established experimental fact (Kirchhoff, 2014; Kirchhoff et al., 2011; Krause, 1973; Li et al., 2020; Murakami and Nobel, 1967; Packer et al., 1965), the appropriateness of the formulation for the function f_s could be checked against observed relative change in the thylakoid volume in response to continuous light intensity variations. Unfortunately, at present, no technology for such measurements is available at these two hierarchies. For this reason, we view our model as exploratory, subject to more rigorous testing in the future. However, at the next hierarchy—the leaf level, which is the most important hierarchy from an application point of view, measurements of J_{PSII} and q are readily available. This paper used these measurements to test the photochemical model developed. The diversity and comprehensiveness of the data set used in the testing (23 C₃ and four C₄ species with temperature, light, O₂ and CO₂ response curves from five countries, collected by www.leafweb. org) are likely unprecedented in a single photosynthetic modelling paper. We think that the likelihood that our model incorrectly represents fundamental redox processes along the electron transport chain, and yet somehow is still able to accurately predict the photochemical J_{PSII} -q relationship across so many species and so broad climates and environmental conditions, is exceedingly small.

A key assumption in our study is that the linear electron transport rate (J_{PSII}) is accurately measured. In reality, J_{PSII} is calculated from the measured photochemical quantum yield of PSII and the assumed values of leaf absorptance (α) in PAR and fraction of absorbed PAR allocated to PSII (β) , which is a common practice in PAM fluorometry. Whereas α can be accurately measured, currently it is difficult to measure β . Although PAM fluorometry typically

9

3633040, 2023, 5, Downloaded from https://onlinelibrary.wiley.com/doi/10.1111/pce.14563, Wiley Online Library on [29/12/2023]. See the Terms and Conditions (https://onlinelibrary.wiley.com/terms-and-conditions) on Wiley Online Library for rules of use; OA articles are governed by the applicable Creative Commons Licenses.

assumes β is a constant (0.5), its precise value depends on state transition (Allen, 2002). An uncertain β would affect the value of J_{PSII} but not the photochemical relationship between J_{PSII} and the fraction of open PSII reaction centres (q) because this relationship is defined by the structural properties of the electron transport chain after PSII. In other words, all redox equations derived in the present study are valid, with or without state transition. This is also true with respect to α . Nevertheless, from Equations (1) and (25), it is clear a different value of β will lead to a proportional change in the calculated J_{PSII} , and when such J_{PSII} is used to optimize for the photochemical parameters, a proportional change in the U parameter will be obtained. However, all other photochemical parameters will remain the same.

We want to point out that our photochemical model facilitates the development of a state transition model. It is known that state transition is regulated by the redox state of the mobile plastoquinone pool (Allen, 2002). Since our photochemical model predicts the redox state of the mobile plastoquinone pool (h_{PQ} or h_{PQH_2} , Equation 28), a state transition model can be formulated with the predicted h_{PO} or h_{POH_2} as an input to further predict β . This state transition model can then be coupled with Equations (1) and (25) so that all photochemical parameters can be estimated from the measured NPQ and q without needing to know J_{PSII} first. Once these parameters are obtained, β and J_{PSII} can be calculated. Furthermore, because state transition and CET of PSI are related, a model for CET of PSI can be formulated with the predicted β as an input. These supplementary models will become part of the overall effort to couple the photochemical model developed in this study, the photophysical model of Gu et al. (2019), and the biochemical model of FvCB for complete modelling of photosynthesis. These ideas will be presented in separate papers to come.

Another uncertainty of the optimized parameters may be caused by the potential presence of CET and pseudo-CET around PSII which, if exist, are currently not represented in our models. However, this uncertainty can be minimized by avoiding measurements made during the first few minutes of dark to light transition within which alternative electron flows around PSII are believed to be significant (Saroussi et al., 2019).

There are many potential applications for the photochemical model developed in this study. For example, it could be used to infer redox reaction parameters, efficiency, and reduction levels of the ETC (e.g., Supporting Information: Table S3 and Figure 8). The model can also be used as a guidance on how the structure of the ETC can be bioengineered to maximize J_{PSII} for a given set of environmental conditions. If a NPQ model is available, then Equation (25) can be coupled with Equation (1) to model essentially all variables in the light reactions of interest at the leaf level and beyond, including SIF emission. If a NPQ model is not available, then Equation (25) should be coupled with Equation (1) and FvCB, together with a state transition and CET model for a complete modelling of photosynthesis from the photophysical reactions to the biochemical reactions.

To conclude, we have now offered an exploratory photochemical model of electron transport that fills a major gap in photosynthesis modelling. This model enables the redox state analyses of electron transport chain with the commonly available PAM fluorometry measurements and the coupling of photophysics and biochemistry for system modelling of the whole photosynthetic machinery. The finding that the oxidation of PQH_2 by Cyt is the bottleneck of the electron transport chain across species may have important implications for genetically improving the efficiency of electron transport and photosynthesis through bioengineering.

ACKNOWLEDGEMENTS

The authors benefited from discussions on photosynthetic electron transport with Drs. Joe Berry, Albert Porcar-Castell and Xinyou Yin. Due to its difficulty, this manuscript in its numerous successive versions was reviewed by at least eight anonymous referees, which led to considerable improvement of the final manuscript. We are grateful to these colleagues. We also thank Dr. Jeff Wood and Ms. Jena Gu for comments on the manuscript. This research is supported by the US Department of Energy (DOE), Office of Science, Biological and Environmental Research Program. ORNL is managed by UT-Battelle, LLC, for DOE under contract DE-AC05-00OR22725. Y. S. and J. H. acknowledge support from NSF Macrosystem Biology (Award 1926488), USDA-NIFA Hatch Fund (1014740), and the Cornell Initiative for Digital Agriculture Research Innovation Fund. B. G. and T. M. acknowledge the support of the Ontario Ministry of Agriculture, Food and Rural Affairs for two OMAFRA-Alliance-T1 Awards (UofG2016-2732 & UG-T1-2021-100932).

DATA AVAILABILITY STATEMENT

The data used in this study is available via www.leafweb.org and tes-sfa. ornl. gov.

ORCID

Lianhong Gu http://orcid.org/0000-0001-5756-8738

Jimei Han http://orcid.org/0000-0001-7466-8511

Yong-Jiang Zhang http://orcid.org/0000-0001-5637-3015

Yang C. Song http://orcid.org/0000-0002-3493-3699

Ying Sun http://orcid.org/0000-0002-9819-1241

REFERENCES

Allen, J.F. (2002) Plastoquinone redox control of chloroplast thylakoid protein phosphorylation and distribution of excitation energy between photosystems: discovery, background, implications. *Photosynthesis Research*, 73, 139–148.

Amarnath, K., Bennett, D.I.G., Schneider, A.R. & Fleming, G.R. (2016) Multiscale model of light harvesting by photosystem II in plants. Proceedings of the National Academy of Sciences, 113, 1156–1161.

Andersson, B. & Anderson, J.M. (1980) Lateral heterogeneity in the distribution of chlorophyll-protein complexes of the thylakoid membranes of spinach chloroplasts. *Biochimica et Biophysica Acta* (BBA)-Bioenergetics, 593, 427–440.

Baker, N.R. (2008) Chlorophyll fluorescence: a probe of photosynthesis in vivo. *Annual Review of Plant Biology*, 59, 89–113.

Beebo, A., Mathai, J.C., Schoefs, B. & Spetea, C. (2013) Assessment of the requirement for aquaporins in the thylakoid membrane of plant chloroplasts to sustain photosynthetic water oxidation. FEBS Letters, 587, 2083–2089.

Blackwell, M., Gibas, C., Gygax, S., Roman, D. & Wagner, B. (1994) The plastoquinone diffusion coefficient in chloroplasts and its

- mechanistic implications. *Biochimica et Biophysica Acta (BBA)-Bioenergetics*, 1183, 533–543.
- Bostick, C.D., Mukhopadhyay, S., Pecht, I., Sheves, M., Cahen, D. & Lederman, D. (2018) Protein bioelectronics: a review of what we do and do not know. Reports on Progress in Physics, 81, 026601.
- Buchanan, B.B. (2016) The carbon (formerly dark) reactions of photosynthesis. *Photosynthesis Research*, 128, 215–217.
- von Caemmerer, S. (2000) Biochemical models of leaf photosynthesis. Collingwood VIC, Australia: CSIRO Publishing, p. 3066.
- Caffarri, S., Tibiletti, T., Jennings, R. & Santabarbara, S. (2014) A comparison between plant photosystem I and photosystem II architecture and functioning. Current Protein & Peptide Science, 15, 296–331.
- Danielsson, R., Albertsson, P.-Å., Mamedov, F. & Styring, S. (2004) Quantification of photosystem I and II in different parts of the thylakoid membrane from spinach. Biochimica et Biophysica Acta (BBA)-Bioenergetics, 1608, 53–61.
- Ebenhöh, O., Houwaart, T., Lokstein, H., Schlede, S. & Tirok, K. (2011) A minimal mathematical model of nonphotochemical quenching of chlorophyll fluorescence. *Biosystems*, 103, 196–204.
- Escoubas, J.M., Lomas, M., LaRoche, J. & Falkowski, P.G. (1995) Light intensity regulation of cab gene transcription is signaled by the redox state of the plastoquinone pool. *Proceedings of the National Academy of Sciences*, 92, 10237–10241.
- Farquhar, G.D., von Caemmerer, S. & Berry, J.A. (1980) A biochemical model of photosynthetic CO₂ assimilation in leaves of C3 species. *Planta*, 149, 78–90.
- Farquhar, G.D., von Caemmerer, S. & Berry, J.A. (2001) Models of photosynthesis. *Plant Physiology*, 125, 42–45.
- Foyer, C.H., Neukermans, J., Queval, G., Noctor, G. & Harbinson, J. (2012) Photosynthetic control of electron transport and the regulation of gene expression. *Journal of Experimental Botany*, 63, 1637–1661.
- Franks, P.J., Buckley, T.N., Shope, J.C. & Mott, K.A. (2001) Guard cell volume and pressure measured concurrently by confocal microscopy and the cell pressure probe. *Plant Physiology*, 125, 1577–1584.
- Geilfus, C.-M. (2018) Chloride: from nutrient to toxicant. Plant and Cell Physiology, 59, 877–886.
- Genty, B., Briantais, J.M. & Baker, N.R. (1989) The relationship between the quantum yield of photosynthetic electron transport and quenching of chlorophyll fluorescence. *Biochimica et Biophysica* Acta (BBA)-General Subjects, 990, 87–92.
- Gu, L., Grodzinski, B., Han, J., Marie, T., Zhang, Y.-J., Song, Y.C. et al. (2022) Granal thylakoid structure and function: explaining an enduring mystery of higher plants. *New Phytologist*, 236, 319–329. Available from: https://doi.org/10.1111/nph.18371
- Gu, L., Han, J., Wood, J.D., Chang, C.Y.Y. & Sun, Y. (2019) Sun-induced Chl fluorescence and its importance for biophysical modeling of photosynthesis based on light reactions. New Phytologist, 223, 1179–1191.
- Haehnel, W. (1984) Photosynthetic electron transport in higher plants. Annual Review of Plant Physiology, 35, 659-693.
- Han, J., Chang, C.Y., Gu, L., Zhang, Y., Walker, A.P., Wen, J. et al. (2022) The physiological basis for estimating photosynthesis from Chla fluorescence. New Phytologist, 234, 1206–1219.
- Han, J., Gu, L., Wen, J. & Sun, Y. (2022) Inferring photosynthetic capacity parameters from solar-induced chlorophyll Fluorescence: key role of the redox state of PSII reaction centers. *Plant, Cell and Environment*, 45, 1298–1314.
- Han, J., Zhang, Y.-J., Sun, Y., Marie, T., Grodzinski, B., Yin, X. et al. (2022) Leafweb: dataset in support of coupled modeling of photophysics, photochemistry, and biochemistry of photosynthesis, December 2022 Release. Oak Ridge National Laboratory, TES SFA, U.S. Department of Energy, Oak Ridge, Tennessee, U.S.A. https://doi. org/10.25581/ornlsfa.027/1887896

- Höhner, R., Pribil, M., Herbstová, M., Lopez, L.S., Kunz, H.-H., Li, M. et al. (2020) Plastocyanin is the long-range electron carrier between photosystem II and photosystem I in plants. Proceedings of the National Academy of Sciences, 117, 15354–15362.
- Johnson, G.N. (2011) Physiology of PSI cyclic electron transport in higher plants. Biochimica et Biophysica Acta (BBA)-Bioenergetics, 1807, 384-389.
- Johnson, J.E. & Berry, J.A. (2021) The role of Cytochrome b₆f in the control of steady-state photosynthesis: a conceptual and quantitative model. *Photosynthesis Research*, 148, 101–136.
- Joliot, P. & Johnson, G.N. (2011) Regulation of cyclic and linear electron flow in higher plants. Proceedings of the National Academy of Sciences, 108, 13317–13322.
- Kamen, M. (1963) Primary processes in photosynthesis. New York: Academic Press.
- Kirchhoff, H. (2014) Structural changes of the thylakoid membrane network induced by high light stress in plant chloroplasts. *Philosophical Transactions of the Royal Society B: Biological Sciences*, 369, 20130225. Available from: https://doi.org/10.1098/rstb. 2013.0225
- Kirchhoff, H., Hall, C., Wood, M., Herbstová, M., Tsabari, O., Nevo, R. et al. (2011) Dynamic control of protein diffusion within the granal thylakoid lumen. *Proceedings of the National Academy of Sciences*, 108. 20248–20253.
- Koochak, H., Puthiyaveetil, S., Mullendore, D.L., Li, M. & Kirchhoff, H. (2019) The structural and functional domains of plant thylakoid membranes. *The Plant Journal*, 97, 412–429.
- Kramer, D.M., Johnson, G., Kiirats, O. & Edwards, G.E. (2004) New fluorescence parameters for the determination of QA redox state and excitation energy fluxes. *Photosynthesis Research*, 79, 209–218.
- Krause, G.H. (1973) The high-energy state of the thylakoid system as indicated by chlorophyll fluorescence and chloroplast shrinkage. *Biochimica et Biophysica Acta (BBA)-Bioenergetics*, 292, 715–728.
- Laisk, A., Eichelmann, H. & Oja, V. (2006) C₃ photosynthesis in silico. Photosynthesis Research, 90, 45–66.
- Laisk, A., Eichelmann, H. & Oja, V. (2015) Oxidation of plastohydroquinone by photosystem II and by dioxygen in leaves. *Biochimica et Biophysica Acta (BBA)-Bioenergetics*, 1847, 565–575.
- Lavergne, J. (1982) Two types of primary acceptors in chloroplasts photosystem II. Photobiochem Photobiophys, 3, 257–285.
- Lazár, D. (2013) Simulations show that a small part of variable chlorophyll a fluorescence originates in photosystem I and contributes to overall fluorescence rise. *Journal of Theoretical Biology*, 335, 249–264.
- Li, M., Mukhopadhyay, R., Svoboda, V., Oung, H.M.O., Mullendore, D.L. & Kirchhoff, H. (2020) Measuring the dynamic response of the thylakoid architecture in plant leaves by electron microscopy. *Plant Direct*, 4(11), e00280. Available from: https://doi.org/10.1002/ pld3.280
- Li, M., Svoboda, V., Davis, G., Kramer, D., Kunz, H.-H. & Kirchhoff, H. (2021) Impact of ion fluxes across thylakoid membranes on photosynthetic electron transport and photoprotection. *Nature Plants*, 7, 979–988.
- Long, S.P. (2003) Gas exchange measurements, what can they tell us about the underlying limitations to photosynthesis? Procedures and sources of error. *Journal of Experimental Botany*, 54, 2393–2401.
- Loriaux, S.D., Avenson, T.J., Welles, J.M., McDermitt, D.K., Eckles, R.D., Riensche, B. et al. (2013) Closing in on maximum yield of chlorophyll fluorescence using a single multiphase flash of sub-saturating intensity. *Plant, Cell & Environment*, 36, 1755–1770.
- Miyake, C., Amako, K., Shiraishi, N. & Sugimoto, T. (2009) Acclimation of tobacco leaves to high light intensity drives the plastoquinone oxidation system—relationship among the fraction of open PSII centers, non-photochemical quenching of Chl fluorescence and the maximum quantum yield of PSII in the dark. *Plant & Cell Physiology*, 50, 730–743.

chloroplasts. Plant & Cell Physiology, 44, 457-462.

- Miyake, C. & Okamura, M. (2003) Cyclic electron flow within PSII protects PSII from its photoinhibition in thylakoid membranes from spinach
- Murakami, S. & Nobel, P.S. (1967) Lipids and light-dependent swelling of isolated spinach chloroplasts. *Plant and Cell Physiology*, 8, 657-671.
- Nawrocki, W.J., Bailleul, B., Picot, D., Cardol, P., Rappaport, F., Wollman, F.-A. et al. (2019) The mechanism of cyclic electron flow. *Biochimica et Biophysica Acta (BBA)-Bioenergetics*, 1860, 433–438.
- Nevo, R., Charuvi, D., Tsabari, O. & Reich, Z. (2012) Composition, architecture and dynamics of the photosynthetic apparatus in higher plants. *The Plant Journal*, 70, 157–176.
- Ohnishi, M., Furutani, R., Sohtome, T., Suzuki, T., Wada, S., Tanaka, S. et al. (2021) Photosynthetic parameters show specific responses to essential mineral deficiencies. *Antioxidants*, 10, 996. Available from: https://doi.org/10.3390/antiox10070996
- Oxborough, K. & Baker, N.R. (1997) Resolving chlorophyll a fluorescence images of photosynthetic efficiency into photochemical and non-photochemical components—calculation of qP and Fv'/Fm' without measuring Fo. *Photosynthesis Research*, 54, 135–142.
- Packer, L., Siegenthaler, P. & Nobel, P.S. (1965) Light-induced volume changes in spinach chloroplasts. *Journal of Cell Biology*, 26, 593–599.
- Porcar-Castell, A. (2011) A high-resolution portrait of the annual dynamics of photochemical and non-photochemical quenching in needles of *Pinus sylvestris*. *Physiologia Plantarum*, 143, 139–153.
- Rantala, M., Rantala, S. & Aro, E.M. (2020) Composition, phosphorylation and dynamic organization of photosynthetic protein complexes in plant thylakoid membrane. *Photochemical & Photobiological Sciences*, 19, 604–619.
- Rochaix, J.D. (2011) Regulation of photosynthetic electron transport. Biochimica et Biophysica Acta (BBA)-Bioenergetics, 1807, 375–383.
- Saroussi, S., Karns, D.A.J., Thomas, D.C., Bloszies, C., Fiehn, O., Posewitz, M.C. et al. (2019) Alternative outlets for sustaining photosynthetic electron transport during dark-to-light transitions. Proceedings of the National Academy of Sciences, 116, 11518-11527.
- Schreiber, U. & Klughammer, C. (2016) Analysis of photosystem I donor and acceptor sides with a new type of Online-Deconvoluting Kinetic LED-Array Spectrophotometer. *Plant Cell Physiology*, 57, 1454–1467.
- Sharkey, T.D. (1985) O₂-insensitive photosynthesis in C₃ plants. Its occurrence and a possible explanation. *Plant Physiology*, 78, 71–75.
- Silverstein, T.P. (2012) Marcus theory: thermodynamics can control the kinetics of electron transfer reactions. *Journal of Chemical Education*, 89, 1159–1167.
- Stirbet, A., Lazár, D., Guo, Y. & Govindjee, G. (2020) Photosynthesis: basics, history and modelling. *Annals of Botany*, 126, 511-537.

- Szabò, I. & Spetea, C. (2017) Impact of the ion transportome of chloroplasts on the optimization of photosynthesis. *Journal of Experimental Botany*, 68, 3115–3128.
- Tikhonov, A.N. (2014) The cytochrome b₆f complex at the crossroad of photosynthetic electron transport pathways. *Plant Physiology and Biochemistry*, 81, 163–183.
- Vehtari, A., Gelman, A. & Gabry, J. (2017) Practical Bayesian model evaluation using leave-one-out cross-validation and WAIC. Statistics and Computing, 27, 1413–1432.
- Vitali, V., Sutka, M., Amodeo, G., Chara, O. & Ozu, M. (2016) The water to solute permeability ratio governs the osmotic volume dynamics in beetroot vacuoles. *Frontiers in Plant Science*, 7, 1388. Available from: https://doi.org/10.3389/fpls.2016.01388
- Wang, B.-X., Tao, M.-J., Ai, Q., Xin, T., Lambert, N., Ruan, D. et al. (2018) Efficient quantum simulation of photosynthetic light harvesting. npj Quantum Information, 4, 52.
- Wilson, K.E., Ivanov, A.G., Öquist, G., Grodzinski, B., Sarhan, F. & Huner, N.P.A. (2006) Energy balance, organellar redox status and acclimation to environmental stress. *Canadian Journal of Botany*, 84, 1355–1370.
- Zhu, X.-G., Govindjee G., Baker, N.R., deSturler, E., Ort, D.R. & Long, S.P. (2005) Chlorophyll a fluorescence induction kinetics in leaves predicted from a model describing each discrete step of excitation energy and electron transfer associated with Photosystem II. *Planta*, 223, 114–133.
- Zhu, X.-G., de Sturler, E. & Long, S.P. (2007) Optimizing the distribution of resources between enzymes of carbon metabolism can dramatically increase photosynthetic rate: a numerical simulation using an evolutionary algorithm. *Plant Physiology*, 145, 513–526.
- Zhu, X.-G., Wang, Y., Ort, D.R. & Long, S.P. (2013) e-Photosynthesis: a comprehensive dynamic mechanistic model of C3 photosynthesis: from light capture to sucrose synthesis. *Plant, Cell & Environment*, 36, 1711–1727.

SUPPORTING INFORMATION

Additional supporting information can be found online in the Supporting Information section at the end of this article.

How to cite this article: Gu, L., Grodzinski, B., Han, J., Marie, T., Zhang, Y.-J., Song, Y. C. et al. (2023) An exploratory steady-state redox model of photosynthetic linear electron transport for use in complete modeling of photosynthesis for broad applications. *Plant, Cell & Environment*, 46, 1540–1561. https://doi.org/10.1111/pce.14563